

## Accepted Manuscript

Synthesis, structural, DFT calculations and biological studies of rhodium and iridium complexes containing azine Schiff-base ligands

Sanjay Adhikari, Dipankar Sutradhar, Samantha L. Shepherd, Roger M. Phillips, Asit K. Chandra, K. Mohan Rao

PII: S0277-5387(16)30218-2  
DOI: <http://dx.doi.org/10.1016/j.poly.2016.06.001>  
Reference: POLY 12039

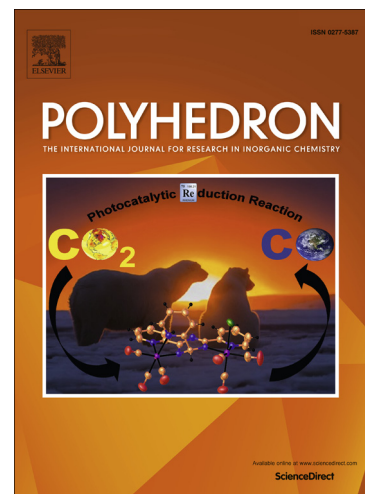
To appear in: *Polyhedron*

Received Date: 4 May 2016

Accepted Date: 1 June 2016

Please cite this article as: S. Adhikari, D. Sutradhar, S.L. Shepherd, R.M. Phillips, A.K. Chandra, K. Mohan Rao, Synthesis, structural, DFT calculations and biological studies of rhodium and iridium complexes containing azine Schiff-base ligands, *Polyhedron* (2016), doi: <http://dx.doi.org/10.1016/j.poly.2016.06.001>

This is a PDF file of an unedited manuscript that has been accepted for publication. As a service to our customers we are providing this early version of the manuscript. The manuscript will undergo copyediting, typesetting, and review of the resulting proof before it is published in its final form. Please note that during the production process errors may be discovered which could affect the content, and all legal disclaimers that apply to the journal pertain.



1 Synthesis, structural, DFT calculations and biological studies of rhodium and  
2 iridium complexes containing azine Schiff-base ligands

3  
4  
5 Sanjay Adhikari<sup>a</sup>, Dipankar Sutradhar<sup>a</sup>, Samantha L. Shepherd<sup>b</sup>, Roger M Phillips<sup>b</sup>,  
6 Asit K. Chandra<sup>a</sup>, K. Mohan Rao<sup>a\*</sup>

7  
8  
9 <sup>a</sup>Centre for Advanced Studies in Chemistry, North-Eastern Hill University,  
10 Shillong 793 022, India.

11 E-mail: [mohanrao59@gmail.com](mailto:mohanrao59@gmail.com)

12 Telephone Number: +91 364 2722620

13 Fax Number: +91 364 2550076

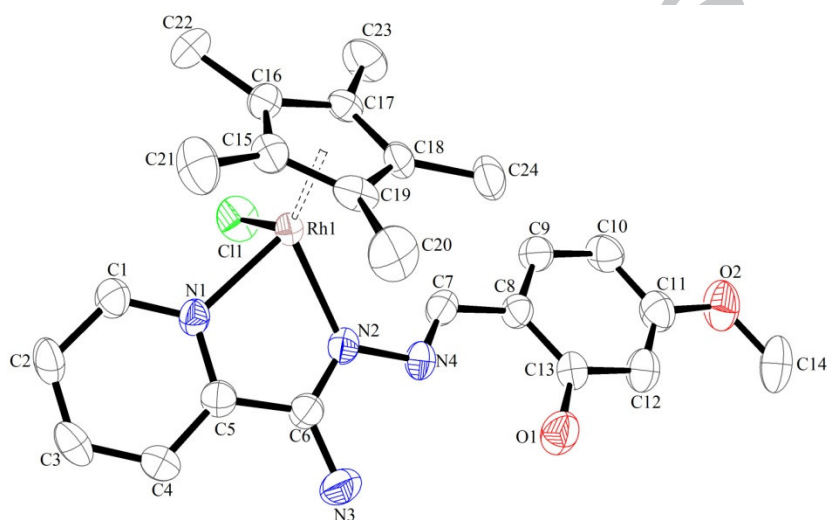
14 <sup>b</sup>Department of Pharmacy, School of Applied Sciences, University of Huddersfield, Huddersfield  
15 HD1 3DH, UK

16

17 **Graphical abstract**

18 Half-sandwich Cp\*Rh(III) and Cp\*Ir(III) complexes have been synthesized with N-N' azine  
19 Schiff-base ligands and characterized by spectroscopic techniques. The molecular structures of  
20 some of the representative complexes have been confirmed by single crystal X-ray analysis.  
21 Chemo-sensitivity activities of the complexes were evaluated against HT-29 (human colorectal  
22 cancer) cell line and non-cancer cell line ARPE-19 (human retinal epithelial cells).

23



24

25

Complex 1

26

27 **Abstract**

28           The reaction of  $[\text{Cp}^*\text{MCl}_2]_2$  ( $\text{M} = \text{Rh}/\text{Ir}$ ) with N-N' azine Schiff-base ligands (L1-L4)  
29 leads to the formation of mononuclear cationic half-sandwich complexes having the general  
30 formula  $[\text{Cp}^*\text{M}(\text{L})\text{Cl}]^+$  (**1–8**), ( $\text{M} = \text{Rh}/\text{Ir}$  and  $\text{L} =$  (2-hydroxy-4-methoxybenzylidene)2-  
31 pyridylamidrazone (L1), (2-hydroxybenzylidene)2-pyridylamidrazone (L2), (1-(2-  
32 hydroxyphenyl)ethylidene)2-pyridylamidrazone (L3) and (1-phenylethylidene)2-  
33 pyridylamidrazone (L4). All these complexes were isolated as their hexafluorophosphate salts  
34 and fully characterized by spectroscopic and analytical techniques. The molecular structure of  
35 complexes (**1**), (**3**), (**4**), (**7**) and (**8**) have been determined by single crystal X-ray crystallographic  
36 studies which displayed the coordination of the ligand to the metal in a bidentate N $\cap$ N fashion  
37 through nitrogen atom of pyridine and one azine nitrogen. The chemo-sensitivity activities of the  
38 complexes were evaluated against HT-29 (human colorectal cancer) cell line and non-cancer cell  
39 line ARPE-19 (human retinal epithelial cells) which revealed that the complexes are moderately  
40 cytotoxic to cancer cells over human cells although complex **5** was the most potent among all the  
41 compounds. Theoretical studies carried out using DFT and TD-DFT at B3LYP level shows good  
42 agreement with the experimental results.

---

43 Keywords: Rhodium, Iridium, Azine Schiff-base ligands, Cytotoxicity

44

## 45 1. Introduction

46 The chemistry of half-sandwich organometallic complexes has evolved as a versatile  
47 subject of research during the past few decades due to its wide application in biological and  
48 medicinal fields [1-4]. Organometallic half-sandwich compounds of the general formula  
49  $[\text{Cp}^*\text{MCl}(\text{LL}')]$  ( $\text{M} = \text{Rh}, \text{Ir}$  and  $\text{LL}' = \text{N},\text{N}$  or  $\text{N},\text{O}$  donor ligands) have been extensively studied  
50 for their cytostatic activity, DNA binding, cellular uptake and as DNA intercalators [5-9].  
51 Rhodium and iridium complexes have also been investigated as an alternative to platinum based  
52 drugs mainly because of their water solubility and lability towards ligand exchange [10, 11].  
53 Recently Therrien *et.al* reported dinuclear dithiolato bridged rhodium and iridium complexes  
54 which exhibit cytotoxicity against human ovarian cancer cells lines (A2780 and A2780cisR)  
55 [12]. C-H activated cyclometallated Rh(III) and Ir(III) complexes can effectively bind to DNA  
56 and protein through electrostatic and hydrophobic interactions [13]. Iridium complexes of  
57 dihydroxybipyridine are active catalysts for homogenous water oxidation under mild reaction  
58 conditions [14]. Rh(III) and Ir(III) polypyridyl complexes exhibits strong antiproliferative  
59 activity towards human cancer cell lines and are also capable of binding to DNA [15]. A number  
60 of half-sandwich Ir(III) complexes have been reported by Sadler *et al* with chelating C, N and  
61 pyridine ligands and N, N donor ligands which showed strong antiproliferative activity [16, 17].

62 Pyridyl azines represent an important class of organic compounds with interesting  
63 properties having wide applications in various areas [18]. Open chain diazine Schiff base ligands  
64 linked by a single N-N bond are of great interest due to its rotational flexibility around the N-N  
65 bond and potential donor sites which can give rise to a rich variety of coordination compounds  
66 with different binding modes [19]. The N-N bridging ligand plays a crucial role in  
67 communicating the metal centers to form mononuclear, dinuclear or polynuclear complexes [20].

68 The diazine ligand has been employed into several transition metal azido and thiocyanato  
69 systems namely Mn(II)-azido, Cd(II)-NCS to obtain several 1D, 2D and 3D polymers which  
70 exhibit interesting magnetic properties [21, 22]. Dinuclear transition metal complexes of Cu, Zn,  
71 Mn and Ni have been reported with bridging N-N diazine ligands which give rise to strong  
72 ferromagnetic and antiferromagnetic coupling [23]. In the recent years our group has reported  
73 many half-sandwich Ru(II), Rh(III) and Ir(III) complexes with azine ligands [24, 25]. In  
74 continuation with our interest of these ligands herein we report four new azine Schiff base  
75 ligands derived from 2-pyridylamidrazone and its corresponding rhodium and iridium half-  
76 sandwich metal complexes. The complexes were tested for their cytotoxic property to selectively  
77 kill HT-29 cancer cell line against normal ARPE-19 cells.

## 78 2. Experimental Section

### 79 2.1. Physical methods and materials

80 All the reagents were purchased from commercial sources and used as received. Starting  
81 materials  $\text{RhCl}_3 \cdot n\text{H}_2\text{O}$ ,  $\text{IrCl}_3 \cdot n\text{H}_2\text{O}$  were purchased from Arora Matthey limited. 2-  
82 cyanopyridine, 2-hydroxybenzaldehyde, 2-hydroxyacetophenone, were obtained from Aldrich,  
83 acetophenone and 2-hydroxy-4-methoxybenzaldehyde were obtained from Alfa-Aesar. The  
84 solvents were purified and dried according to standard procedures [26]. All the reactions were  
85 carried out under normal conditions. The starting precursor metal complexes  $[\text{Cp}^*\text{MCl}_2]_2$  (M =  
86 Rh/Ir) were prepared according to the literature methods [27]. Infrared spectra were recorded on  
87 a Perkin-Elmer 983 spectrophotometer by using KBr pellets in the range of  $400\text{-}4000\text{ cm}^{-1}$ .  $^1\text{H}$   
88 NMR spectra were recorded on a Bruker Avance II 400 MHz spectrometer using  $\text{DMSO-d}_6$  and  
89  $\text{CDCl}_3$  as solvents. Absorption spectra were recorded on a Perkin-Elmer Lambda 25 UV/Visible  
90 spectrophotometer in the range of 200-800 nm at room temperature in acetonitrile. Elemental

91 analyses of the complexes were performed on a Perkin-Elmer 2400 CHN/S analyzer. Mass  
92 spectra were recorded using Q-ToF APCI-MS instrument (model HAB 273). All these  
93 mononuclear metal complexes were synthesized and characterized by using FT-IR,  $^1\text{H}$  NMR,  
94 UV-Vis, and Single-crystal X-ray diffraction techniques.

## 95 2. 2. *Single-crystal X-ray structures analyses*

96 The orange crystals of complexes (1), (3), (7) and (8) were obtained by slow diffusion of  
97 hexane into acetone or DCM solution and yellow crystals of complex (4) was obtained by  
98 diffusing hexane into DCM solution. Single crystal X-ray diffraction data for all the complexes  
99 (1), (3) (4), (7) and (8) were collected on a Oxford Diffraction Xcalibur Eos Gemini  
100 diffractometer at 293 K using graphite monochromated Mo-K $\alpha$  radiation ( $\lambda = 0.71073 \text{ \AA}$ ). The  
101 strategy for the data collection was evaluated using the CrysAlisPro CCD software. Crystal data  
102 were collected by standard “phi-omega scan” techniques and were scaled and reduced using  
103 CrysAlisPro RED software. The structures were solved by direct methods using SHELXS-97  
104 and refined by full-matrix least squares with SHELXL-97 refining on  $F^2$  [28, 29]. The positions  
105 of all the atoms were obtained by direct methods. Metal atoms in the complex were located from  
106 the E-maps and non-hydrogen atoms were refined anisotropically. The hydrogen atoms bound to  
107 the carbon were placed in geometrically constrained positions and refined with isotropic  
108 temperature factors, generally 1.2  $U_{\text{eq}}$  of their parent atoms. Crystallographic and structure  
109 refinement details for the complexes are summarized in Table 1, and selected bond lengths and  
110 bond angles are presented in Table S1. Figures 1-3 were drawn with ORTEP3 program. Figure 4  
111 and Figures S3-S6 were drawn with MERCURY3.6 program [30].

## 112 2.3. *Biological studies*

113 All complexes (**1-8**) were dissolved in DMSO at 100 mM and stored at -20 °C until  
114 needed. The complexes were tested against cancer cell line HT-29 (human colorectal cancer),  
115 and one non-cancer cell line ARPE-19 (human retinal epithelial cells). Cells were seeded into 96  
116 well plates at  $1 \times 10^3$  cells per well and incubated at 37 °C in a CO<sub>2</sub> enriched (5%), humidified  
117 atmosphere overnight to adhere. The cells were exposed to a range of drug concentrations in the  
118 range of 0-100 μM for four days before cell survival was determined using the MTT assay [31].  
119 To each well MTT (0.5 mg/ml) was added and was further incubated at 37 °C for 4 h. After this  
120 the MTT was removed from each well and the formazan crystals formed were dissolved in 150  
121 μM DMSO. The absorbance of the resulting solution was recorded at 550 nm using an ELISA  
122 spectrophotometer. The percentage of cell inhibition was calculated by dividing the absorbance  
123 of treated cell by the control value absorbance (exposed to 0.1 % DMSO). The results were  
124 expressed in terms of IC<sub>50</sub> values (concentration required to kill 50 % cell) and all studies were  
125 performed in triplicate. The results were also expressed in terms of a 'selectivity index' defined  
126 as the IC<sub>50</sub> of the non-cancer cell line ARPE divided by the IC<sub>50</sub> of cancer cell lines [32]. Values  
127 greater than 1 demonstrate that the compound is preferentially active against tumor cell  
128 compared to normal cell lines.

#### 129 2.4. *Computational methodology*

130 All the electronic structure calculations of the metal complexes (**1-8**) were carried out  
131 using the Gaussian 09 suite of program [33]. The geometries of the rhodium and iridium  
132 complexes were optimized in the gas phase employing the DFT-based B3LYP method with 6-  
133 31G\*\* basis set for (H, C, N, O, Cl, F and P atoms and LANL2DZ [34, 35] for (Rh and Ir)  
134 atoms. Harmonic frequency calculations were carried out at the same level of theory to ensure  
135 that the optimized geometries were true minima on the potential energy surface (PES). Natural



136 Bond Orbital (NBO) analysis [36] was used to obtain the charge distribution on individual atoms  
137 and the d-orbital occupations of the metal present in the complexes. Time dependent-Density  
138 Functional Theory (TD-DFT) [37] has been employed to evaluate the absorption spectra and the  
139 electronic transitions of the metal complexes. In order to incorporate the effect of the solvent  
140 around the molecule, the Polarizable Continuum Model (PCM) [38] was used in TD-DFT  
141 calculations. The percentage contribution of molecular orbital analysis was carried out using  
142 Chemissian software package [39].

#### 143 **2.4. General procedure for preparation of ligands 1-4**

144 **2.4.1.** The azine Schiff base ligands (L1-L4) were prepared by two step procedure.

145 In the first step 2-pyridylamidrazone was prepared, by following a reported procedure  
146 [40]. 2-cyanopyridine and hydrazine hydrate were dissolved and stirred in absolute ethanol  
147 overnight to give 2-pyridylamidrazone as yellow crystalline solid which was used in the next  
148 step without further purification (Scheme-1). In the second step (5 mmol) of aldehyde or ketone  
149 and 2-pyridylamidrazone (5 mmol) was refluxed in 10 ml ethanol for 5 hours (Scheme-2). The  
150 products obtained after cooling the solution were filtered off washed with cold methanol and  
151 diethyl ether and dried in vacuum.

152 Data for ligands (L1-L4)

#### 153 **2.4.2. (2-hydroxy-4-methoxybenzylidene)2-pyridylamidrazone (L1)**

154 Color: Yellow needles; Yield: 88%; IR (KBr,  $\text{cm}^{-1}$ ): 3487(s), 3380(s), 3333(m), 2964(m),  
155 1627(s), 1587(m), 1566(m), 1394(m), 1340(s);  $^1\text{H}$  NMR (400 MHz,  $\text{CDCl}_3$ ):  $\delta$  = 11.82 (s, 1H,  
156 OH), 8.60 (s, 1H,  $\text{CH}_{(\text{imine})}$ ), 8.57 (d, 1H,  $J$  = 4.0 Hz,  $\text{CH}_{(\text{py})}$ ), 8.34 (d, 1H,  $J$  = 8.0 Hz,  $\text{CH}_{(\text{py})}$ ),  
157 7.76 (t, 1H,  $\text{CH}_{(\text{py})}$ ), 7.35 (t, 1H,  $\text{CH}_{(\text{py})}$ ), 7.20 (d, 2H,  $J$  = 8.0 Hz,  $\text{CH}_{(\text{Ar})}$ ), 6.46-6.50 (m, 3H,  $\text{NH}_2$ ,  
158  $\text{CH}_{(\text{Ar})}$ ), 3.80 (s, 3H, OMe); HRMS-APCI ( $m/z$ ): 271.11  $[\text{M}+\text{H}]^+$ ; UV-Vis {Acetonitrile,  $\lambda_{\text{max}}$ ,

159 nm ( $\epsilon/10^4 \text{ M}^{-1} \text{ cm}^{-1}$ ): 218 (0.84), 314 (0.68), 342 (0.92), 355 (0.94); Anal. Calc. for  $\text{C}_{14}\text{H}_{14}\text{N}_4\text{O}_2$   
160 (270.29): C, 62.21; H, 5.22; N, 20.73. Found: C, 62.36; H, 5.35; N, 20.86%.

161 2.4.3. (2-hydroxybenzylidene)2-pyridylamidrazone (L2)

162 Color: Yellow needles; Yield: 92%; IR (KBr,  $\text{cm}^{-1}$ ): 3477(s), 3363(s), 3340(s), 3043(m), 1626(s),  
163 1576(m), 1567(m), 1473(m), 1337(m);  $^1\text{H}$  NMR (400 MHz,  $\text{CDCl}_3$ ):  $\delta$  = 11.61 (s, 1H, OH), 8.59  
164 (s, 1H,  $\text{CH}_{(\text{imine})}$ ), 8.54 (d, 1H,  $J$  = 4.0 Hz,  $\text{CH}_{(\text{py})}$ ), 8.28 (d, 1H,  $J$  = 8.0 Hz,  $\text{CH}_{(\text{py})}$ ), 7.74 (t, 1H,  
165  $\text{CH}_{(\text{py})}$ ), 7.33 (t, 1H,  $\text{CH}_{(\text{py})}$ ), 7.24-7.27 (m, 3H,  $\text{NH}_2$ ,  $\text{CH}_{(\text{Ar})}$ ), 6.96 (d, 1H,  $J$  = 8.0 Hz,  $\text{CH}_{(\text{Ar})}$ ),  
166 6.87 (t, 2H,  $\text{CH}_{(\text{Ar})}$ ); HRMS-APCI ( $m/z$ ): 241.10  $[\text{M}+\text{H}]^+$ ; UV-Vis {Acetonitrile,  $\lambda_{\text{max}}$ , nm ( $\epsilon/10^4$   
167  $\text{M}^{-1} \text{ cm}^{-1}$ ): 219 (0.84), 247 (0.55), 349 (1.30), 361 (1.29); Anal. Calc. for  $\text{C}_{13}\text{H}_{12}\text{N}_4\text{O}$  (240.26):  
168 C, 64.99; H, 5.03; N, 23.32. Found: C, 65.12; H, 5.18; N, 23.44%.

169 2.4.4. (1-(2-hydroxyphenyl)ethylidene)2-pyridylamidrazone (L3)

170 Color: Yellow crystalline solid; Yield: 95%; IR (KBr,  $\text{cm}^{-1}$ ): 3482(s), 3339(s), 3056(m),  
171 3003(m), 1615(s), 1562(m), 1507(m), 1300(m);  $^1\text{H}$  NMR (400 MHz,  $\text{CDCl}_3$ ):  $\delta$  = 13.73 (s, 1H,  
172 OH), 8.59 (d, 1H,  $J$  = 4.0 Hz,  $\text{CH}_{(\text{py})}$ ), 8.36 (d, 1H,  $J$  = 8.0 Hz,  $\text{CH}_{(\text{py})}$ ), 7.79 (t, 1H,  $\text{CH}_{(\text{py})}$ ), 7.58  
173 (t, 1H,  $\text{CH}_{(\text{py})}$ ), 7.21-7.28 (m, 3H,  $\text{NH}_2$ ,  $\text{CH}_{(\text{Ar})}$ ), 6.98 (d, 2H,  $J$  = 8.0 Hz,  $\text{CH}_{(\text{Ar})}$ ), 6.89 (t, 1H,  
174  $\text{CH}_{(\text{Ar})}$ ), 2.62 (s, 3H,  $\text{CH}_3$ ); HRMS-APCI ( $m/z$ ): 255.12  $[\text{M}+\text{H}]^+$ ; UV-Vis {Acetonitrile,  $\lambda_{\text{max}}$ , nm  
175 ( $\epsilon/10^4 \text{ M}^{-1} \text{ cm}^{-1}$ ): 217 (1.21), 303 (0.74), 344 (0.95); Anal. Calc. for  $\text{C}_{14}\text{H}_{14}\text{N}_4\text{O}$  (254.29): C,  
176 66.13; H, 5.55; N, 22.03. Found: C, 66.25; H, 5.68; N, 22.21%.

177 2.4.5. (1-phenylethylidene)2-pyridylamidrazone (L4)

178 Color: Yellow crystalline solid; Yield: 92%; IR (KBr,  $\text{cm}^{-1}$ ): 3450(s), 3331(s), 3056(m),  
179 3009(m), 1604(s), 1568(m), 1445(m), 1362(m);  $^1\text{H}$  NMR (400 MHz,  $\text{CDCl}_3$ ):  $\delta$  = 8.58 (d, 1H,  $J$   
180 = 4.0 Hz,  $\text{CH}_{(\text{py})}$ ), 8.23 (d, 1H,  $J$  = 8.0 Hz,  $\text{CH}_{(\text{py})}$ ), 7.71 (t, 1H,  $\text{CH}_{(\text{py})}$ ), 7.30 (t, 1H,  $\text{CH}_{(\text{py})}$ ), 7.21-  
181 7.28 (m, 3H,  $\text{NH}_2$ ,  $\text{CH}_{(\text{Ar})}$ ), 6.93 (m, 3H,  $\text{CH}_{(\text{Ar})}$ ), 6.89 (t, 1H,  $\text{CH}_{(\text{Ar})}$ ), 2.39 (s, 3H,  $\text{CH}_3$ ); HRMS-

182 APCI (m/z): 239.13 [M+H]<sup>+</sup>; UV-Vis {Acetonitrile,  $\lambda_{\max}$ , nm ( $\epsilon/10^4$  M<sup>-1</sup> cm<sup>-1</sup>): 225 (0.21), 327  
183 (0.29); Anal. Calc. for C<sub>14</sub>H<sub>14</sub>N<sub>4</sub> (238.29): C, 70.57; H, 5.92; N, 23.51. Found: C, 70.72; H, 6.03;  
184 N, 23.62%.

### 185 2.5. General procedure for preparation of metal complexes (1-8)

186 A mixture of metal precursor [Cp\*MCl<sub>2</sub>]<sub>2</sub> (M = Rh/Ir) (0.1 mmol), azine Schiff-base ligands (L1-  
187 L4) (0.2 mmol) and 2.5 equivalents of NH<sub>4</sub>PF<sub>6</sub> in dry methanol (10 ml) was stirred at room  
188 temperature for 8 hours (Scheme-3). The solvent was evaporated under reduced pressure, and the  
189 residue was dissolved in dichloromethane and filtered over celite to remove excess salt. The  
190 filtrate was reduced to 2 ml and diethyl ether was added to induce precipitation. The yellow  
191 colored precipitate, which formed, was filtered and washed with diethyl ether and dried in  
192 vacuum.

#### 193 2.5.1. [Cp\*Rh(L1)Cl]PF<sub>6</sub> (1)

194 Yield: 56 mg (40%); IR (KBr, cm<sup>-1</sup>): 3460(m), 3237(m), 2926(w), 1630(s), 1595(m), 1296(m),  
195 846(s); <sup>1</sup>H NMR (400 MHz, CDCl<sub>3</sub>):  $\delta$  = 10.5 (s, 1H, OH), 9.02 (s, 1H, CH<sub>(imine)</sub>), 8.76 (d, 1H, *J*  
196 = 4.0 Hz, CH<sub>(py)</sub>), 8.54 (d, 1H, *J* = 4.0 Hz, CH<sub>(py)</sub>), 8.13 (t, 1H, CH<sub>(py)</sub>), 7.76 (t, 1H, CH<sub>(py)</sub>), 7.41  
197 (d, 1H, *J* = 8.0 Hz, CH<sub>(Ar)</sub>), 7.38 (s, 2H, NH<sub>2</sub>), 6.53 (d, 1H, *J* = 8.0 Hz, CH<sub>(Ar)</sub>), 6.50 (s, 1H,  
198 CH<sub>(Ar)</sub>), 3.81 (s, 3H, OMe), 1.58 (s, 15H, CH<sub>(Cp\*)</sub>); HRMS-APCI (m/z): 507.12 [M-PF<sub>6</sub>-HCl]<sup>+</sup>;  
199 UV-Vis {Acetonitrile,  $\lambda_{\max}$ , nm ( $\epsilon/10^4$  M<sup>-1</sup> cm<sup>-1</sup>): 233 (0.98), 277 (0.57), 352 (0.42); Anal.  
200 Calc. for C<sub>24</sub>H<sub>29</sub>ClF<sub>6</sub>N<sub>4</sub>O<sub>2</sub>PRh (688.84): C, 41.85; H, 4.24; N, 8.13. Found: C, 41.96; H, 4.16; N,  
201 8.23%.

#### 202 2.5.2. [Cp\*Ir(L1)Cl]PF<sub>6</sub> (2)

203 Yield: 70 mg (45%); IR (KBr, cm<sup>-1</sup>): 3447(m), 3241(m), 2925(m), 1630(s), 1610(m), 1293(m),  
204 846(s); <sup>1</sup>H NMR (400 MHz, CDCl<sub>3</sub>):  $\delta$  = 10.4 (s, 1H, OH), 9.02 (s, 1H, CH<sub>(imine)</sub>), 8.77 (d, 1H, *J*

205 = 4.0 Hz, CH<sub>(py)</sub>), 8.51 (d, 1H, *J* = 4.0 Hz, CH<sub>(py)</sub>), 8.17 (t, 1H, CH<sub>(py)</sub>), 7.78 (t, 1H, CH<sub>(py)</sub>), 7.42  
206 (d, 1H, *J* = 8.0 Hz, CH<sub>(Ar)</sub>), 7.39 (s, 2H, NH<sub>2</sub>), 6.56 (d, 1H, *J* = 8.0 Hz, CH<sub>(Ar)</sub>), 6.54 (s, 1H,  
207 CH<sub>(Ar)</sub>), 3.87 (s, 3H, OMe), 1.62 (s, 15H, CH<sub>(Cp\*)</sub>); HRMS-APCI (*m/z*): 597.18 [M-PF<sub>6</sub>-HCl]<sup>+</sup>;  
208 UV-Vis {Acetonitrile, λ<sub>max</sub>, nm (ε/10<sup>4</sup> M<sup>-1</sup> cm<sup>-1</sup>)}: 266 (0.36), 347 (0.29); Anal. Calc. for  
209 C<sub>24</sub>H<sub>29</sub>ClF<sub>6</sub>N<sub>4</sub>O<sub>2</sub>PIr (778.14): C, 37.04; H, 3.76; N, 7.20. Found: C, 37.19; H, 3.89; N, 7.31%.

### 210 2.5.3. [Cp\*Rh(L2)Cl]PF<sub>6</sub> (3)

211 Yield: 52 mg (39%); IR (KBr, cm<sup>-1</sup>): 3422(m), 3310(w), 2923(w), 1636(s), 1603(m), 1457(m),  
212 845(s); <sup>1</sup>H NMR (400 MHz, CDCl<sub>3</sub>): δ = 10.1 (s, 1H, OH), 9.11 (s, 1H, CH<sub>(imine)</sub>), 8.78 (d, 1H, *J*  
213 = 4.0 Hz, CH<sub>(py)</sub>), 8.49 (d, 1H, *J* = 8.0 Hz, CH<sub>(py)</sub>), 8.14 (t, 2H, CH<sub>(py)</sub>), 7.78 (t, 1H, CH<sub>(Ar)</sub>), 7.60  
214 (d, 1H, *J* = 8.0 Hz, CH<sub>(Ar)</sub>), 7.38 (s, 2H, NH<sub>2</sub>), 6.92-7.01 (m, 2H, CH<sub>(Ar)</sub>), 1.58 (s, 15H, CH<sub>(Cp\*)</sub>);  
215 HRMS-APCI (*m/z*): 477.12 [M-PF<sub>6</sub>-HCl]<sup>+</sup>; UV-Vis {Acetonitrile, λ<sub>max</sub>, nm (ε/10<sup>4</sup> M<sup>-1</sup> cm<sup>-1</sup>)}:  
216 235 (1.55), 283 (0.79), 348 (1.00); Anal. Calc. for C<sub>23</sub>H<sub>27</sub>ClF<sub>6</sub>N<sub>4</sub>OPRh (658.81): C, 41.93; H,  
217 4.13; N, 8.50. Found: C, 42.08; H, 4.25; N, 8.68%.

### 218 2.5.4. [Cp\*Ir(L2)Cl]PF<sub>6</sub> (4)

219 Yield: 52 mg (34%); IR (KBr, cm<sup>-1</sup>): 3479(s), 3329(s), 2924(w), 1642(s), 1618(m), 1602(m),  
220 842(s); <sup>1</sup>H NMR (400 MHz, CDCl<sub>3</sub>): δ = 10.1 (s, 1H, OH), 9.13 (s, 1H, CH<sub>(imine)</sub>), 8.80 (d, 1H, *J*  
221 = 4.0 Hz, CH<sub>(py)</sub>), 8.56 (d, 1H, *J* = 8.0 Hz, CH<sub>(py)</sub>), 8.18 (t, 2H, CH<sub>(py)</sub>), 7.80 (t, 1H, CH<sub>(Ar)</sub>), 7.64  
222 (d, 1H, *J* = 8.0 Hz, CH<sub>(Ar)</sub>), 7.40 (s, 2H, NH<sub>2</sub>), 6.99-7.35 (m, 2H, CH<sub>(Ar)</sub>), 1.63 (s, 15H, CH<sub>(Cp\*)</sub>);  
223 HRMS-APCI (*m/z*): 567.17 [M-PF<sub>6</sub>-HCl]<sup>+</sup>; UV-Vis {Acetonitrile, λ<sub>max</sub>, nm (ε/10<sup>4</sup> M<sup>-1</sup> cm<sup>-1</sup>)}:  
224 291 (0.62), 344 (0.78); Anal. Calc. for C<sub>23</sub>H<sub>27</sub>ClF<sub>6</sub>N<sub>4</sub>OPIr (748.12): C, 36.93; H, 3.64; N, 7.49.  
225 Found: C, 37.11; H, 3.83; N, 7.62%.

### 226 2.5.5. [(Cp\*Rh(L3)Cl]PF<sub>6</sub> (5)

227 Yield: 58 mg (43%); IR (KBr,  $\text{cm}^{-1}$ ): 3452(s), 3318(s), 2924(m), 1648(s), 1600(m), 1566(m),  
228 1489(m), 842(s);  $^1\text{H}$  NMR (400 MHz, DMSO- $d_6$ ):  $\delta$  = 12.5 (s, 1H, OH), 8.96 (d, 1H,  $J$  = 4.0 Hz,  
229  $\text{CH}_{(\text{py})}$ ), 8.33-8.38 (m, 3H,  $\text{CH}_{(\text{py})}$ ), 7.91 (t, 1H,  $\text{CH}_{(\text{Ar})}$ ), 7.86 (d, 1H,  $J$  = 8.0 Hz,  $\text{CH}_{(\text{Ar})}$ ), 7.48 (t,  
230 1H,  $J$  = 8.0 Hz,  $\text{CH}_{(\text{Ar})}$ ), 7.01-7.06 (m, 3H,  $\text{NH}_2$ ,  $\text{CH}_{(\text{Ar})}$ ), 2.48 (s, 3H,  $\text{CH}_3$ ), 1.59 (s, 15H,  
231  $\text{CH}_{(\text{Cp}^*)}$ ); HRMS-APCI (m/z): 491.14  $[\text{M-PF}_6\text{-HCl}]^+$ ; UV-Vis {Acetonitrile,  $\lambda_{\text{max}}$ , nm ( $\epsilon/10^{-4} \text{ M}^{-1}$   
232  $\text{cm}^{-1}$ )}: 229 (0.95), 268 (0.59), 332 (0.32); Anal. Calc. for  $\text{C}_{24}\text{H}_{29}\text{ClF}_6\text{N}_4\text{OPRh}$  (672.84): C,  
233 42.84; H, 4.34; N, 8.33. Found: C, 42.98; H, 4.26; N, 8.48%.

#### 234 2.5.6. $[\text{Cp}^*\text{Ir}(\text{L}3)\text{Cl}]\text{PF}_6$ (6)

235 Yield: 65 mg (42%); IR (KBr,  $\text{cm}^{-1}$ ): 3460(m), 3237(m), 2926(w), 1630(s), 1595(m), 1296(m),  
236 846(s), 3456(m), 3369(m), 2925(m), 1649(s), 1618(m), 1598(m), 1306(m), 845(s);  $^1\text{H}$  NMR  
237 (400 MHz, DMSO- $d_6$ ):  $\delta$  = 12.3 (s, 1H, OH), 8.94 (d, 1H,  $J$  = 4.0 Hz,  $\text{CH}_{(\text{py})}$ ), 8.44 (d, 1H,  $J$  =  
238 4.0 Hz,  $\text{CH}_{(\text{py})}$ ), 8.35 (t, 2H,  $\text{CH}_{(\text{py})}$ ), 7.90 (t, 1H,  $\text{CH}_{(\text{Ar})}$ ), 7.86 (d, 1H,  $J$  = 8.0 Hz,  $\text{CH}_{(\text{Ar})}$ ), 7.48 (t,  
239 1H,  $\text{CH}_{(\text{Ar})}$ ), 7.01-7.06 (m, 3H,  $\text{NH}_2$ ,  $\text{CH}_{(\text{Ar})}$ ), 2.46 (s, 3H,  $\text{CH}_3$ ), 1.58 (s, 15H,  $\text{CH}_{(\text{Cp}^*)}$ ); HRMS-  
240 APCI (m/z): 581.19  $[\text{M-PF}_6\text{-HCl}]^+$ ; UV-Vis {Acetonitrile,  $\lambda_{\text{max}}$ , nm ( $\epsilon/10^{-4} \text{ M}^{-1} \text{ cm}^{-1}$ )}: 209  
241 (1.27), 263 (0.66), 330 (0.36); Anal. Calc. for  $\text{C}_{24}\text{H}_{29}\text{ClF}_6\text{N}_4\text{OPIr}$  (762.15): C, 37.82; H, 3.84; N,  
242 7.35. Found: C, 37.96; H, 3.96; N, 7.44%.

#### 243 2.5.7. $[(\text{Cp}^*\text{Rh}(\text{L}4)\text{Cl}]\text{PF}_6$ (7)

244 Yield: 54 mg (41%); IR (KBr,  $\text{cm}^{-1}$ ): 3441(s), 3137(m), 2961(w), 1640 (s), 1593(m), 1464(m),  
245 841(s);  $^1\text{H}$  NMR (400 MHz, DMSO- $d_6$ ):  $\delta$  = 8.96 (d, 1H,  $J$  = 4.0 Hz,  $\text{CH}_{(\text{py})}$ ), 8.33-8.37 (m, 2H,  
246  $\text{CH}_{(\text{py})}$ ), 7.88 (t, 1H,  $\text{CH}_{(\text{py})}$ ), 7.81 (d, 1H,  $J$  = 8.0 Hz,  $\text{CH}_{(\text{Ar})}$ ), 7.46 (t, 1H,  $\text{CH}_{(\text{Ar})}$ ), 7.23-7.28 (m,  
247 2H,  $\text{CH}_{(\text{Ar})}$ ), 6.97-7.02 (m, 3H,  $\text{NH}_2$ ,  $\text{CH}_{(\text{Ar})}$ ), 2.47 (s, 3H,  $\text{CH}_3$ ), 1.59 (s, 15H,  $\text{CH}_{(\text{Cp}^*)}$ ); HRMS-  
248 APCI (m/z): 511.12  $[\text{M-PF}_6]^+$ ; UV-Vis {Acetonitrile,  $\lambda_{\text{max}}$ , nm ( $\epsilon/10^{-4} \text{ M}^{-1} \text{ cm}^{-1}$ )}: 229 (1.37),

249 265 (0.37), 400 (0.22); Anal. Calc. for  $C_{24}H_{29}ClF_6N_4PRh$  (656.84): C, 43.89; H, 4.45; N, 8.53.

250 Found: C, 44.02; H, 4.39; N, 8.61%.

### 251 2.5.8. $[Cp^*Ir(L4)Cl]PF_6$ (**8**)

252 Yield: 65 mg (43%); IR (KBr,  $cm^{-1}$ ): 3458(s), 3383(s), 2922(m), 1643(s), 1603(m), 1567(m),

253 1447(m), 844(s);  $^1H$  NMR (400 MHz, DMSO- $d_6$ ):  $\delta$  = 8.97 (d, 1H,  $J$  = 4.0 Hz,  $CH_{(py)}$ ), 8.31-8.34

254 (m, 2H,  $CH_{(py)}$ ), 7.85 (t, 1H,  $CH_{(py)}$ ), 7.79 (d, 1H,  $J$  = 8.0 Hz,  $CH_{(Ar)}$ ), 7.44 (t, 1H,  $CH_{(Ar)}$ ), 7.19-

255 7.23 (m, 2H,  $CH_{(Ar)}$ ), 6.99-7.03 (m, 3H,  $NH_2$ ,  $CH_{(Ar)}$ ), 2.46 (s, 3H,  $CH_3$ ), 1.59 (s, 15H,  $CH_{(Cp^*)}$ );

256 HRMS-APCI (m/z): 601.17  $[M-PF_6]^+$ ; UV-Vis {Acetonitrile,  $\lambda_{max}$ , nm ( $\epsilon/10^{-4} M^{-1} cm^{-1}$ )}: 256

257 (0.53), 361 (0.20); Anal. Calc. for  $C_{24}H_{29}ClF_6N_4PIr$  (746.15): C, 38.63; H, 3.92; N, 7.51. Found:

258 C, 38.74; H, 4.03; N, 7.63%.

## 259 3. Results and discussion

### 260 3.1. Synthesis of ligands and complexes

261 The azine Schiff-base ligands (L1-L4) were prepared by the reaction of 2-  
262 pyridylamidrazone and the respective aldehyde or ketone in absolute ethanol medium. The  
263 complexes (**1-8**) were synthesized by the reaction of Rh/Ir metal precursors with the azine  
264 Schiff-base ligands. The cationic complexes were isolated with  $PF_6$  counter ion. All these metal  
265 complexes were obtained in good yields and are yellow in color. They are stable in air as well as  
266 in solid state, and are non-hygroscopic. These complexes are soluble in common organic  
267 solvents such as dichloromethane, acetonitrile and acetone but insoluble in diethyl ether and  
268 hexane. All the synthesized ligands and complexes were fully characterized by spectroscopic  
269 techniques.

### 270 3.2. Spectroscopic characterization of ligands

271 The infrared spectra of the free ligand shows characteristic stretching frequencies for  
272  $\text{NH}_2$ , OH, C=N and C=C groups. The  $\text{NH}_2$  and OH stretching frequencies for the azine ligand  
273 appeared in the range of 3300-3500  $\text{cm}^{-1}$ . The C=C and C=N stretching frequencies were  
274 observed in the range of 1550-1626  $\text{cm}^{-1}$ . The proton NMR spectra of the ligands displayed  
275 signals in the range of 7.30-8.57 ppm assignable to the protons of the pyridine ring. The imine  
276 protons for L1 and L2 are located at 8.60 and 8.59 ppm respectively. The methoxy proton signal  
277 was observed as a singlet for L1 at 3.80 ppm. The methyl protons of L3 and L4 were observed as  
278 a singlet at 2.62 and 2.39 ppm respectively. The hydroxyl proton resonance for the ligands  
279 appeared in the range of 11.5-11.9 ppm. The aromatic protons of the ligand appeared as doublet,  
280 triplet and multiplet in the range of 6.21-7.29 ppm. The  $[\text{M}+\text{H}]^+$  molecular ion peak for the  
281 ligands are shown in the experimental section which are found to be in good agreement with the  
282 expected range. The electronic spectra of the free ligands are shown in (Figure S1). The  
283 electronic spectra of the free ligands show absorption bands in the range of 210-360 nm. The  
284 band in the range of 210-250 nm can be assigned as  $\pi$ - $\pi^*$  and  $n$ - $\pi^*$  transition. The band around  
285 300-370 nm is due to the intermolecular charge transfer transition within the whole molecule  
286 [41].

### 287 3.3. Spectroscopic characterization of complexes

288 The IR spectra of the complexes show sharp bands around 842-846  $\text{cm}^{-1}$  due to the P-F  
289 stretching frequency of the counter ion [42]. The OH and  $\text{NH}_2$  stretching vibrations in the  
290 complexes were found around 3300-3500  $\text{cm}^{-1}$ . The retaining of the OH and  $\text{NH}_2$  stretching  
291 frequencies indicates that they are not involved in bonding to the metal center. The strong  
292 absorption band for  $\nu_{\text{C}=\text{N}}$  around 1630-1650  $\text{cm}^{-1}$  at higher wave numbers as compared to the free

293 ligand around 1615-1626  $\text{cm}^{-1}$  suggest that the coordination to the metal occurs through the  
294 imine and pyridine nitrogen.

295 The proton NMR spectra of the metal complexes show that the ligand resonance signals  
296 are shifted downfield as compared to that of the free ligand. These signals are shifted downfield  
297 because of the ligand coordination to the metal atom. The imine proton signal was observed in  
298 the range of 9.0-9.13 ppm for complexes (1-4). The hydroxyl proton resonance for the  
299 complexes appeared in the range of 10.1-12.5 ppm respectively. The appearance of the hydroxyl  
300 proton signal indicates that the hydroxyl group is not involved in bonding to the metal atom. The  
301 pyridine ring protons also showed downfield signals comprising of doublet and triplet in the  
302 range of 7.75-8.96 ppm. The  $\text{NH}_2$  protons were observed as a singlet for complexes (1-4) in the  
303 range of 7.35-7.37 ppm respectively. The methoxy proton resonance for complexes (1 and 2)  
304 appeared as a singlet at 3.81 and 3.83 ppm. The aromatic proton signals for complexes appeared  
305 in the range of 6.50-7.86 ppm as doublet, triplet and multiplet. The methyl proton signal for  
306 complexes (5-8) appeared as a singlet around 2.46-2.48 ppm respectively. In addition to the  
307 signals for the ligand protons, a sharp singlet was observed for all the complexes between 1.58-  
308 1.63 ppm respectively corresponding to the methyl protons of the  $\text{Cp}^*$  ring. In the mass spectra  
309 of the complexes (1-6) the peaks at  $m/z$ : 507.12,  $m/z$ : 597.18,  $m/z$ : 477.12,  $m/z$ : 567.17,  $m/z$ :  
310 491.13 and  $m/z$ : 581.20 can be assigned as  $[\text{M-PF}_6\text{-HCl}]^+$  ion peaks respectively. Whereas, the  
311 mass spectra of the complex 7 and 8 displayed molecular ion peaks at  $m/z$ : 511.12 and 601.17  
312 which corresponds to the  $[\text{M-PF}_6]^+$  ion.

313 The electronic spectra of the complexes were recorded in acetonitrile at  $10^{-4}$  M  
314 concentration at room temperature and the plot is shown in (Figure S2). The electronic spectra of  
315 complexes display two absorption band in the higher energy region around 210-330 nm. The



316 bands in the higher energy UV region can be assigned as ligand centered or intra ligand  $\pi$ - $\pi^*$  and  
317  $n$ - $\pi^*$  transition. The Rh(III) and Ir(III) complexes provides filled  $d\pi$  ( $t_{2g}$ ) orbitals which can  
318 interact with low lying  $\pi^*$  orbitals (C=N) of the ligand. The band in the lower energy region  
319 around 345-405 nm can be assigned as Rh ( $d\pi$ ) or Ir ( $d\pi$ ) to  $\pi^*$  ligand metal to ligand charge  
320 transfer (MLCT) transition [43].

#### 321 3.4. *Molecular structures of complexes*

322 The molecular structures of some of the respective complexes have been elucidated by  
323 single crystal X-ray analysis. Suitable single crystals were attached to a glass fibre and  
324 transferred into the Oxford Diffraction Xcalibur Eos Gemini diffractometer. The crystallographic  
325 details and structure refinement details are summarized in Table 1. The geometrical parameters  
326 around the metal atom involving ring centroid are listed in Table S1. In all these complexes the  
327 ligand is coordinated to the metal atom in a similar manner with N $\cap$ N binding mode. Complex  
328 (1) and (8) crystallized in triclinic system with space group P $\bar{1}$ . Complex (8) crystallized with  
329 one PF<sub>6</sub> and one chloride counter ion. Complex (3) and (4) crystallized in monoclinic system  
330 with space group P2<sub>1</sub>/c whereas complex (7) crystallized in monoclinic system with space group  
331 P2<sub>1</sub>.

332 All these complexes display a typical three-legged piano stool geometry around the metal  
333 center with coordination sites occupied by one chloride group, two  $\sigma$  bonded nitrogen atoms  
334 from chelating azine ligand and the pentamethylcyclopentadienyl (Cp\*) ring in  $\eta^5$  manner. The  
335 metal atom in all these complexes is situated in a pseudo-octahedral arrangement with the azine  
336 ligand coordinating through the pyridine and azine nitrogen atoms forming a five membered  
337 metallocycle. In complexes (1), (3), (4) and (7) the M-N bond length {2.088(5), 2.099(3),  
338 2.098(4) and 2.102(4) Å} from pyridine is comparatively shorter than the azine nitrogen-metal

339 distances {2.135(5), 2.116(3), 2.105(4) and 2.159(4) Å}, which are similar to those, reported  
340 with similar complexes [24, 44]. However in complex (8) the metal-nitrogen distance from  
341 pyridine {2.102(5) Å} is comparatively larger than azine nitrogen-metal distance, which is  
342 {2.096(5) Å}. The C=N bond length of the coordinated nitrogen in complex (1), (3), (4) and (8)  
343 is longer than that of the uncoordinated C=N (Table S1) which could be due to the back bonding  
344 of electron from metal ( $d\pi$ ) to  $\pi^*$  orbital of the ligand. But in complex (7), a reverse pattern has  
345 been observed where the C=N bond length of the coordinated nitrogen {1.346(7) Å} is shorter  
346 than uncoordinated C=N {1.358(7) Å} bond. The average M-C distances are {2.159 (1), 2.1534  
347 (3), 2.1616 (4), 2.1528 (7) and 2.1726 (8) Å} while the distance between the metal to Cp\*  
348 centroid ring is in the range of 1.758–1.793 Å respectively. The M-Cl bond lengths {2.3976(15)  
349 (1), 2.4172(9) (3), 2.4190(12) (4), 2.4242(16) (7) and 2.4220(17) (8) shows no significant  
350 differences and is comparable to previously reported values (Table 1) [45-48]. The bite angle  
351 N(1)-Rh(1)-N(2) values are 75.10(19) (1), 75.09(11) (3), and 75.44(17) (7) whereas in complex  
352 (4) and (8) the bite angle values are N(1)-Ir(1)-N(2) values are 74.99(14) (4) and 75.26(18)  
353 respectively which probably indicates an inward bending of the coordinated pyridyl and azine  
354 group [49]. The bond angles N(1)-M-Cl(1) and N(2)-M-Cl(1) in complexes are comparable to  
355 the piano stool arrangement about the metal atom and is comparable to reported values for  
356 closely related systems [50-52]. Further the crystal packing in complex (1) is stabilized by weak  
357 intermolecular hydrogen bonding C-H $\cdots$ O (2.702 Å) between the hydrogen atom from methoxy  
358 group and oxygen atom of the hydroxyl group and C-H $\cdots$ Cl (2.793 Å) interaction between CH<sub>3</sub>  
359 group of Cp\* and chloride atom (Figure S3). These interactions play a significant role in the  
360 formation of supramolecular motifs.

361 On the other hand in the crystal structure of complex (3) and (4) two types of  
362 intramolecular hydrogen bonding has been observed; the first one between the uncoordinated  
363 nitrogen atom of the azine linkage with the hydrogen atom of the hydroxyl group  $O-H\cdots N$   
364 (1.916 and 1.908 Å) and the second between the hydrogen atom from  $NH_2$  and uncoordinated  
365 azine nitrogen atom  $N-H\cdots N$  (2.323 and 2.328 Å) (Figure 4). The selected hydrogen bonding  
366 distances and angles for complex (3) and (4) are given in (Table 2). Also the crystal packing in  
367 complex (3) and (4) is further stabilized by two different  $C-H\cdots Cl$  interaction between the Cl  
368 atom attached to metal M (where M = Rh/Ir) with hydrogen atom of pyridine ring and  $NH_2$   
369 (Figure S4). Complex (7) shows  $C-H\cdots\pi$  (2.832 and 2.937 Å) interactions between the methyl  
370 hydrogen atom and  $Cp^*$  moiety and between pyridine ring and hydrogen atom of  $Cp^*$  group  
371 respectively (Figure S5). Interestingly the crystal packing in complex (8) leads to a dimeric unit  
372 via intermolecular  $C-H\cdots Cl$  interaction between the chloride counter ion and hydrogen atom  
373 from pyridine ring,  $NH_2$  and  $Cp^*$  group (Figure S6).

### 374 3.5. Chemosensitivity studies

375 The complexes (1-8) were tested for their cytotoxicity against cancer cell line HT-29  
376 (human colorectal cancer), and non-cancer cell line ARPE-19 (human retinal epithelial cells).  
377 The response of the cell lines HT-29 to the test complexes and cisplatin (1-8) is presented in  
378 graphical form in Figure 5 and in tabular form in Table 3. All the complexes tested were found to  
379 be active against HT-29 cancer cell line ( $IC_{50} < 30 \mu M$ ). Complex (5) was the most potent among  
380 all the complexes with ( $IC_{50}$  value of  $96.93 \pm 5.31 \mu M$ ). However all the complexes were less  
381 potent than cisplatin ( $IC_{50}$  value of  $0.25 \pm 0.11 \mu M$  against HT-29). The selectivity index (SI)  
382 defined as the ratio of  $IC_{50}$  values in ARPE19 cells divided by the  $IC_{50}$  value of cancer cell line  
383 demonstrates that all the complexes are effective against cancer cell with SI values ranging from

384 1.01 to 2.11 (Table S2). Moreover although complex (5) showed more selectivity than other  
385 complexes for HT-29 cancer cell, however its selectivity was significantly lower than cisplatin  
386 where SI value is 25.64 (Figure 6).

### 387 3.6. *Optimized geometry*

388 The comparison of the geometric parameters (selected bond lengths and bond angles) of  
389 the optimized structures and the crystal structures of the complexes (1, 3, 4, 7 and 8) are listed in  
390 Table S3. All the metal complexes are found to be closed shell structures. The calculated bond  
391 lengths and the bond angles of the complexes are in good agreement with the experimental data  
392 indicating the reliability of the theoretical method (B3LYP/6-31G\*\*/LanL2DZ) used in the  
393 present study. It should be noted that for complexes (3, 4, 7 and 8), the M(1)-N(2) (where M =  
394 Rh/Ir) bond length is slightly longer than the M(1)-N(1) bond length whereas for complex (1), a  
395 reverse pattern has been observed (Table S3).

### 396 3.7. *Charge distribution*

397 The charges on the individual atoms for the metal complexes obtained from NBO  
398 analysis are listed in Table S4. The charges on the Rh atom in the complexes (1), (3), (5) and (7)  
399 are 0.136, 0.200, 0.216 and 0.214 e whereas the charges on Ir for complexes (2), (4), (6) and (8)  
400 are 0.186, 0.252, 0.268 and 0.214 e respectively. These NBO charges on Rh and Ir are  
401 comparatively lower than their formal charge of +3 which suggests that the ligand transfers their  
402 negative charge to the respective rhodium and iridium metal on complex formation. In metal  
403 complexes (1-8), the charge on Cl ranges between -0.439 e (Complex-1) to -0.394 e (Complex-  
404 4). In isolated ligands, the charge on N(1) ranges between -0.416 and -0.417 e whereas for N(2)  
405 it ranges between -0.324 e and -0.348 e. It should be noted that for isolated ligands as well as for  
406 complexes (1-8), the negative charges on N(1) (-0.385, -0.381, -0.372, -0.373, -0.369, -0.398, -

0.368 and -0.373 e) are slightly higher than the charges on N(2) (-0.258, -0.253, -0.284, -0.283, -0.305, -0.297, -0.311 and -0.305 e). On complex formation, the negative charge on the N(1) and N(2) reduces slightly giving an indication of the charge transfer on Rh and Ir in metal complexes. The population of the 4d ( $4d_{xy}$ ,  $4d_{xz}$ ,  $4d_{yz}$ ,  $4d_{x^2-y^2}$  and  $4d_z^2$ ) orbital of Rh complexes and 5d orbital of Ir complexes are shown in Table S5. The orbital occupations of each orbital ( $nd_{xy}$ ,  $nd_{xz}$ ,  $nd_{yz}$ ,  $nd_{x^2-y^2}$  and  $nd_z^2$ ) for all the complexes are comparatively higher in rhodium complexes than iridium complexes. In free Rh(III) and Ir(III) state, the population of  $nd_{xy}$ ,  $nd_{xz}$  and  $nd_{yz}$  are 2.0, 2.0 and 2.0 e and the other two orbitals remain vacant. But on complex formation, the population on  $nd_{xy}$ ,  $nd_{xz}$  and  $nd_{yz}$  orbital gets reduced whereas the  $nd_{x^2-y^2}$  and  $nd_z^2$  orbitals gain some population as indicated in Table S5. For most of the complexes, the population of 4d and 5d orbital containing the same ligand follow similar pattern of filling, except for the complexes containing ligand L1 where the  $nd_{xz}$  orbital population is slightly lower and  $nd_{x^2-y^2}$  is higher as compared to the other complexes.

### 3.8. Frontier molecular orbitals and absorption spectra

The molecular orbital representation of the complexes along with their HOMO, LUMO energies and HOMO-LUMO energy gaps are shown in Figure 7. The HOMO-LUMO energy gap can be used as an important parameter in analyzing the chemical reactivity and kinetic stability of a molecule. This energy gap is also related to the hardness/softness of a chemical species [53]. The lower HOMO-LUMO energy gap is a suitable condition where a molecule can be excited easily and thereby increasing its reactivity and decreasing its kinetic stability whereas higher energy gap can lead to more kinetic stability but less reactivity. The HOMO-LUMO energy gaps for all the complexes (**1-8**) are found to be 3.20, 2.98, 3.63, 3.46, 3.61, 3.60, 3.68 and 3.59 eV respectively. The gap is slightly lower for the iridium complexes as compared to rhodium

430 complexes containing the same ligand indicating the reactivity of Ir complexes over the  
431 complexes containing Rh metal. The % contribution of molecular orbital analysis as shown in  
432 Table S6, predicts that the most percentage of HOMO is located on the ligand itself except for  
433 complex (2) and (8) where as it is mostly present on the Ir metal. On the other hand, LUMO is  
434 located on the ligand for complexes (1) (about 97%), (2) (91%), (4) (89%), (6) (92%) and (8)  
435 (69%) whereas for complexes (3) (40%), (5) (35%) and (7) (38%), it is located on the Rh metal.

436 The electronic absorption spectra were calculated using the TD-DFT method in  
437 acetonitrile solvent employing PCM model. The calculated and the experimental absorption data,  
438 HOMO-LUMO energy gaps, and the character of electronic transitions are listed in Table 4. The  
439 H→L transitions for complexes (1), (4) and (6) occurring at 417, 444 and 441 nm corresponds to  
440 ILCT character, for complexes (2) and (8) at 463 and 440 nm corresponds to MLCT character  
441 whereas for complexes (3), (5) and (7) at 532, 519 and 518 nm corresponds to LMCT character.  
442 These MLCT character can be assigned for  $d\pi(M)\rightarrow\pi^*(L)$  transitions whereas the ILCT  
443 character are for  $\pi\rightarrow\pi^*$  transitions. It should be noted that all LMCT transitions are occurring at  
444 higher wavelength regions (i.e. > 500 nm). In good agreement with the experimental data, the  
445 TD-DFT calculations shows few MLCT transitions at 358 nm complex (2), 332 nm, complex  
446 (4), 334 nm complex (6) and 372, 358 nm complex (8). However, in the range between 340-400  
447 nm, few LMCT, ILCT and LLCT transitions have also been observed (Table 4).

#### 448 4. Conclusion

449 In summary, we have synthesized four new azine Schiff-base ligands and its rhodium and  
450 iridium half-sandwich complexes. All these complexes and ligands were full characterized by  
451 various spectroscopic techniques. The ligands under study preferably bind to the metal in a  
452 bidentate N∩N fashion using pyridine and one azine nitrogen atom. Our attempt to synthesize

453 dinuclear rhodium and iridium complexes with NN' and NO bonding was however unsuccessful  
454 irrespective of molar ratio of metal to ligand where as in the presence of base, it leads to  
455 decomposition of the reaction. These complexes possess some important intramolecular and  
456 intermolecular hydrogen bonding and also possess some weak non-covalent interactions,  
457 particularly C-H $\cdots$ Cl and C-H $\cdots$  $\pi$  interactions. Chemosensitivity activity of the complexes  
458 against HT-29 cancer cell demonstrates that the complexes are active however complex (5) was  
459 found to be the most potent among all other complexes. Theoretical studies reveal that the  
460 HOMO-LUMO energy gap is lower for iridium complexes indicating better reactivity over the  
461 rhodium complexes. TD-DFT calculations were carried out in order to evaluate the electronic  
462 transitions occurring in the metal complexes, which are in good agreement with the experimental  
463 results. The charge distribution analysis (using NBO analysis) of these complexes helps to  
464 understand how the charges on nitrogen atom (which are coordinating to the metal) are  
465 delocalized on complex formation. Especially, the NBO charges, on rhodium and iridium  
466 confirm that the ligands transfer their negative charge to the respective metal on complex  
467 formation. The lower HOMO-LUMO energy gap leads to greater chemical reactivity but lesser  
468 kinetic stability and vice versa. Furthermore, the nature of HOMO and LUMO illustrate the  
469 electronic origin of the lowest energy transition and the resulting electronic reorganization.  
470 Moreover, the molecular orbital analysis was helpful to understand and locate the % contribution  
471 of HOMO and LUMO on different fragments of the complexes, which is otherwise not possible  
472 to predict from experimental data.

#### 473 **Acknowledgements**

474 Sanjay Adhikari and Dipankar Sutradhar thanks UGC, New Delhi, India for providing financial  
475 assistance in the form of university fellowship (UGC-Non-Net). We thank DST-PURSE

476 SCXRD, NEHU-SAIF, Shillong, India for providing Single crystal X-ray analysis and other  
477 spectral studies. AKC thanks Computer centre, NEHU, for computational facilities.

#### 478 **Supplementary material**

479 CCDC 1477976 (1), 1477977 (3), 1477978 (4), 1477979 (7) and 1477980 (8) contains  
480 the supplementary crystallographic data for this paper. These data can be obtained free of charge  
481 via [www.ccdc.cam.ac.uk/data\\_request/cif](http://www.ccdc.cam.ac.uk/data_request/cif), by e-mailing [data\\_request@ccdc.cam.ac.uk](mailto:data_request@ccdc.cam.ac.uk), or by  
482 contacting The Cambridge Crystallographic Data Centre, 12, Union Road, Cambridge CB2 1EZ,  
483 UK; Fax: +44 1223 336033.

484

#### 485 **References**

- 486 [1] G. Gasser, I. Ott, N. Metzler-Nolte, *J. Med. Chem.* 54 (2011) 3.
- 487 [2] L. Ronconi, P.J. Sadler, *Coord. Chem. Rev.* 251 (2007) 1633.
- 488 [3] Y.K. Yan, M. Melchart, A. Habtemariam, P.J. Sadler, *Chem. Commun.* (2005) 4764.
- 489 [4] B. Therrien, *Coord. Chem. Rev.* 253 (2009) 493.
- 490 [5] U. Sliwinska, F.P. Pruchnik, S. Ulaszewski, M. Latocha, D. Nawrocka-Musial,  
491 *Polyhedron* 29 (2010) 1653.
- 492 [6] M.A. Scharwitz, I. Ott, Y. Geldmacher, R. Gust, W.S. Sheldrick, *J. Organomet. Chem.*  
493 693 (2008) 2299.
- 494 [7] M.A. Nazif, J.-Amade Bangert, I. Ott, R. Gust, R. Stoll, W.S. Sheldrick, *J. Biol. Inorg.*  
495 *Chem.* 103 (2009) 1405.
- 496 [8] M. Gras. B. Therrien, G. Suss-Fink, A. Casini, F. Edafe, P.J. Dyson, *J. Organomet.*  
497 *Chem.* 695 (2010) 1119.



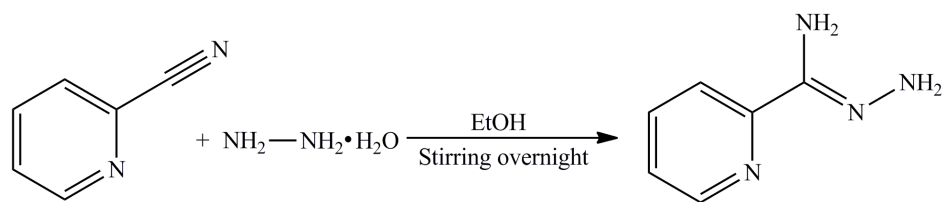
- 498 [9] Y. Geldmacher, M. Oleszak, W.S. Sheldrick, *Inorg. Chim. Acta* 393 (2012) 84.
- 499 [10] R. Bieda, I. Ott, M. Dobroschke, A. Prokop, R. Gust, W.S. Sheldrick, *J. Biol. Inorg.*  
500 *Chem.* 103 (2009) 698.
- 501 [11] Z. Liu, P.J. Sadler, *Acc. Chem. Res.* 47 (2014) 1174.
- 502 [12] G. Gupta, A. Garci, B.S. Murray, P.J. Dyson, G. Fabre, P. Trouillas, F. Giannini, J.  
503 Furrer, G. Suss-Fink, B. Therrien, *Dalton Trans.* 42 (2013) 15457.
- 504 [13] S. Mukhopadhyay, R.K. Gupta, R.P. Paitandi, N.K. Rana, G. Sharma, B. Koch, L.K.  
505 Rana, M.S. Hundal, D.S. Pandey, *Organometallics* 34 (2015) 4491.
- 506 [14] J. De Pasquale, I. Nieto, L.E. Reuther, C.J. H-Gervasoni, J.J. Paul, V. Mochalin. M.  
507 Zeller, C.M. Thomas, A.W. Addison, E.T. Papish, *Inorg. Chem.* 52 (2013) 9175.
- 508 [15] Y. Geldmacher, K. Splith, I. Kitanovic, H. Alborzina, S. Can, R. Rubbiani, M.A. Nazif,  
509 P. Wefelmeier, A. Prokop, I. Ott, S. Wolfl, I. Neundorf, W.S. Sheldrick, *J. Biol. Inorg.*  
510 *Chem.* 17 (2012) 631.
- 511 [16] Z. Liu, I. Romero-Canelon, A. Habtemariam, G.J. Clarkson, P.J. Sadler, *Organometallics*  
512 33 (2014) 5324.
- 513 [17] Z. Liu, A. Habtemariam, A.M. Pizarro, S.A. Fletcher, A. Kisova, O. Vrana, L. Salassa,  
514 P.C.A. Bruijninx, G.J. Clarkson, V. Brabec, P.J. Sadler, *J. Med. Chem.* 54 (2011) 3011.
- 515 [18] J. Safari, S. Gandomi-Ravandi, *RSC Adv.* 4 (2014) 46224.
- 516 [19] Z. Xu, L.K. Thompson, D.O. Miller, *Inorg. Chem.* 36 (1997) 3985.
- 517 [20] M. Ghedini, A.M.M. Lanfredi, F. Neve, A. Tiripicchio, *J. Chem. Soc. Chem. Commun.*  
518 (1987) 847.
- 519 [21] E.-Q. Gao, S.-Q. Bai, Y.-F. Yue, Z.-M. Wang, C.-H. Yan, *Inorg. Chem.* 42 (2003) 3642.
- 520 [22] Y.-F. Yue, C.-J. Fang, E.-Q. Gao, C. He, S.-Q. Bai, S. Xu, C.-H. Yan, *J. Mol. Struct.* 875

- 521 (2008) 80.
- 522 [23] Z. Xu, L.K. Thompson, D.A. Black, C. Ralph, D.O. Miller, M.A. Leech, J.A.K. Howard,  
523 J. Chem. Soc., Dalton Trans. (2001) 2042.
- 524 [24] K.T. Prasad, G. Gupta, A.V. Rao, B. Das, K.M. Rao, Polyhedron 28 (2009) 2649.
- 525 [25] G. Gupta, S. Gloria, S.L. Nongbri, B. Therrien, K.M. Rao, J. Organomet. Chem. 696  
526 (2011) 2014.
- 527 [26] D.D. Perrin, W.L.F. Armarego, Purification of Laboratory Chemicals, fourth ed.,  
528 Butterworths Heinemann, London, 1996.
- 529 [27] C. White, A. Yates, P.M. Maitlis, D.M. Heinekey, Inorg. Synth. 29 (2007) 228.
- 530 [28] G.M. Sheldrick, Acta Crystallogr. Sect. A 64 (2008) 112.
- 531 [29] G.M. Sheldrick Acta Crystallogr. Sect. C 71 (2015) 3.
- 532 [30] L.J. Farrugia, J. Appl. Crystallogr. 32 (1999) 837.
- 533 [31] R.M. Phillips, P.B. Hulbert, M.C. Bibby, N.R. Sleight, J.A. Double, Br. J. Cancer.  
534 65 (1992) 359.
- 535 [32] R.A. Kaner, S.J. Allison, A.D. Faulkner, R.M. Phillips, D.I. Roper, S.L. Shepherd, D.H.  
536 Simpson, N.R. Waterfield, P. Scott, Chem. Sci. 7 (2016) 951.
- 537 [33] M.J. Frisch et al., GAUSSIAN 09, Revision C.01, Gaussian Inc, Walling-ford, CT, 2009.
- 538 [34] A.D. Becke, J. Chem. Phys. 98 (7) (1993) 5648.
- 539 [35] C. Lee, W. Yang, R.G. Parr, Phys. Rev. B 37 (2) (1988) 785.
- 540 [36] E. Cancès, B. Mennucci, J. Tomasi, J. Chem. Phys. 107 (1997) 3032.
- 541 [37] A.E. Reed, L.A. Curtiss, F. Weinhold, Chem. Rev. 88 (1988) 899.
- 542 [38] M.E. Casida, in: J.M. Seminario (Ed.), Recent Developments and Applications in Modern  
543 Density Functional Theory, Theoretical and Computational Chemistry, vol. 4, Elsevier,  
544 Amsterdam, 1996.

- 545 [39] L. Skripnikov, Chemissian v4.36, A computer program to analyse and visualise quantum-  
546 chemical calculations, 2015.
- 547 [40] F. Weldon, L. Hammarstrom, E. Mukhtar, R. Hage, E. Gunneweg, J.G. Haasnoot, J.  
548 Reedijk, W.R. Browne, A.L. Guckian, J.G. Vos, *Inorg. Chem.* 43 (2004) 4471.
- 549 [41] C.U. Dueke-Eze, T.M. Fasina, M.J. Mphahlele, *Asian J. Chem.* 25 (2013) 8505.
- 550 [42] S.D. Dwivedi, A.K. Singh, S.K. Singh, S. Sharma, M. Chandra, D.S. Pandey, *Eur. J.*  
551 *Inorg. Chem.* (2008) 5666.
- 552 [43] P. Govindaswamy, Y.A. Mozharivskyj, K.M. Rao, *Polyhedron* 24 (2005) 1710.
- 553 [44] D.L. Davies, J. Fawcett, R. Krafczyk, D.R. Russell, *J. Organomet. Chem.* 581 (1997)  
554 545.
- 555 [45] P. Chellan, K.M. Land, A. Shokar, A. Au, S.H. An, D. Taylor, P.J. Smith, T. Riedel, P.J.  
556 Dyson, K. Chibale, G.S. Smith, *Dalton Trans.* 43, (2014) 513.
- 557 [46] G. Gupta, G. Sharma, B. Koch, S. Park, S.S. Lee, J. Kim, *New.J.Chem.* 37 (2013) 2573.
- 558 [47] K.S. Singh, Y.A. Mozharivskyj, C. Thone, M.R. Kollipara, *J. Organomet. Chem.* 690  
559 (2005) 3720.
- 560 [48] N.R. Palepu, S.L. Nongbri, J.R. Premkumar, A.K. Verma, K. Bhattacharjee, S.R. Joshi,  
561 S. Forbes, Y.A. Mozharivskyj, R. Thounaojam, K. Aguan, M. R. Kollipara, *J. Biol. Inorg.*  
562 *Chem.* 20 (2015) 619.
- 563 [49] S.K. Singh, M. Chandra, D.S. Pandey, M.C. Puerta, P. Valerga, *J. Organomet. Chem.* 689  
564 (2004), 3612.
- 565 [50] R. Payne, P. Govender, B. Therrien, C.M. Clavel, P.J. Dyson, G.S. Smith, *J. Organomet.*  
566 *Chem.* 729 (2013) 20.
- 567 [51] A.P. Walsh, W.W. Brennessel, W.D. Jones, *Inorg. Chim. Acta* 407 (2013) 131.

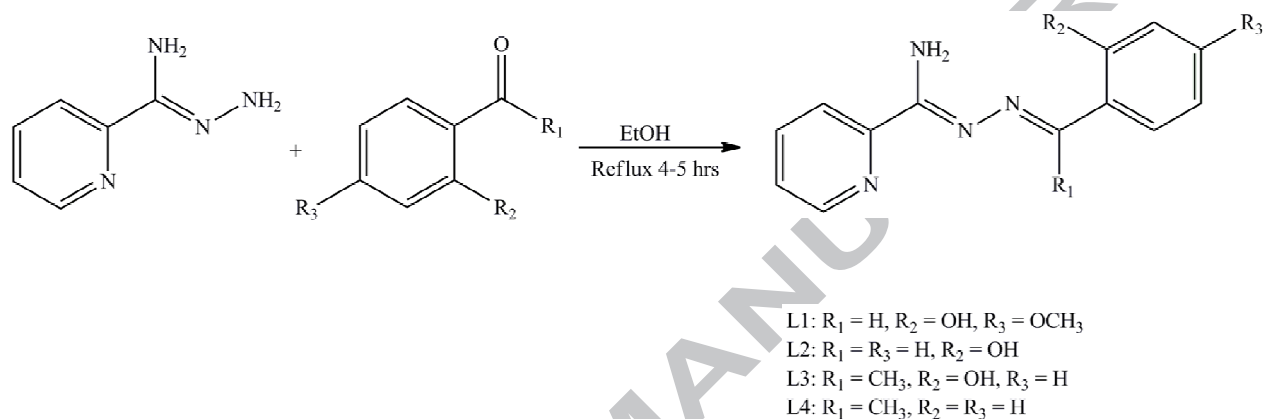
- 568 [52] M. Kalidasan, S.H. Forbes, Y. Mozharivskyj, M.R. Kollipara, *Inorg. Chim. Acta* 421  
569 (2014) 218.
- 570 [52] Y. Hanifehpour, B. Mirtamizdoust, S.W. Joo, *J Inorg Organomet Polym.* 22 (2012) 916.

ACCEPTED MANUSCRIPT

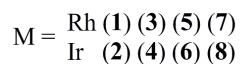
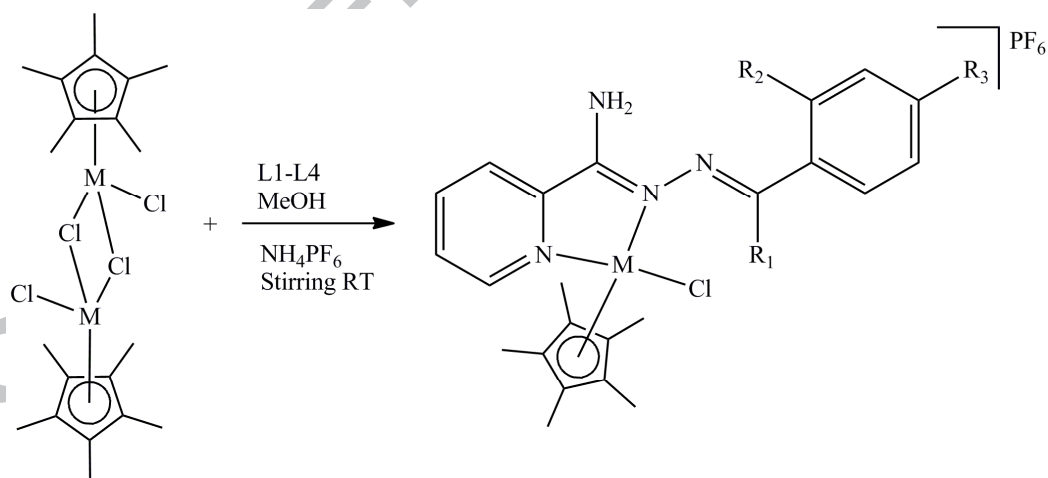


Scheme-1 Synthesis of 2-pyridylamidrazone

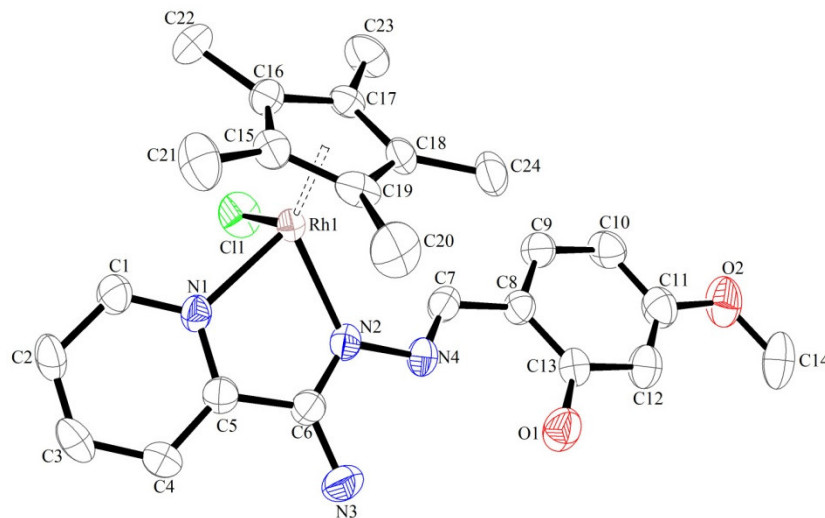
573



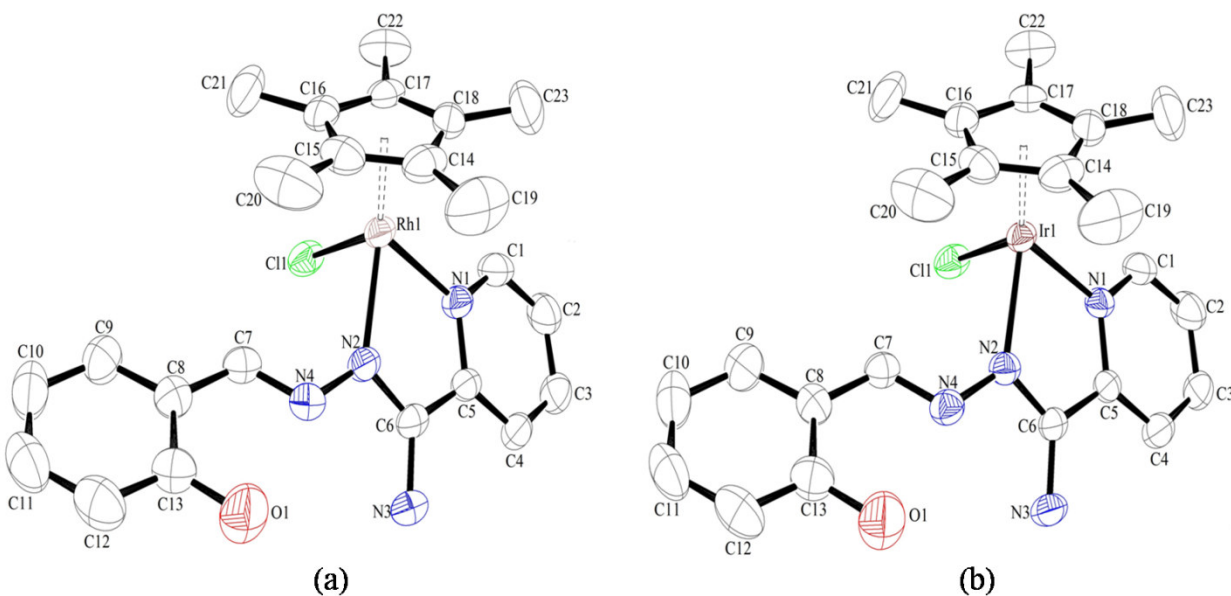
Scheme-2 Preparation of ligands (L1-L4)



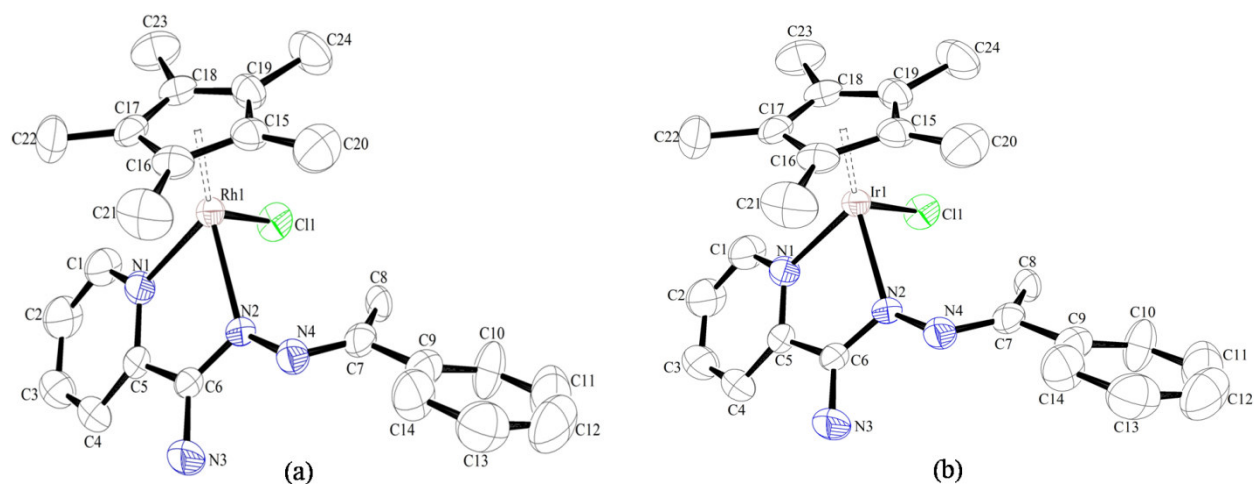
Scheme-3 Preparation of metal complexes (1-8)



579  
 580 **Figure 1** ORTEP diagram of complex  $[\text{Cp}^*\text{RhCl}(\text{L1})\text{Cl}]\text{PF}_6$  (**1**) with 50% probability thermal  
 581 ellipsoids. Hydrogen atoms and counter ions are omitted for clarity.



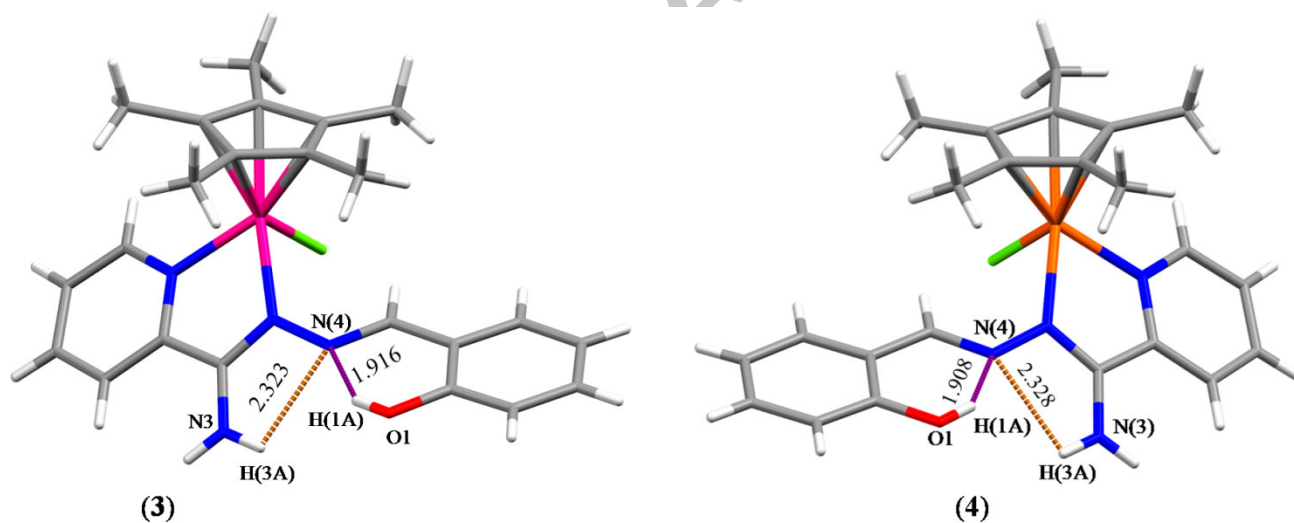
582  
 583 **Figure 2** (a) ORTEP diagram of complex  $[\text{Cp}^*\text{RhCl}(\text{L2})\text{Cl}]\text{PF}_6$  (**3**) and (b) ORTEP diagram of  
 584 complex  $[\text{Cp}^*\text{IrCl}(\text{L2})\text{Cl}]\text{PF}_6$  (**4**) with 50% probability thermal ellipsoids. Hydrogen atoms and  
 585 counter ions are omitted for clarity.



586

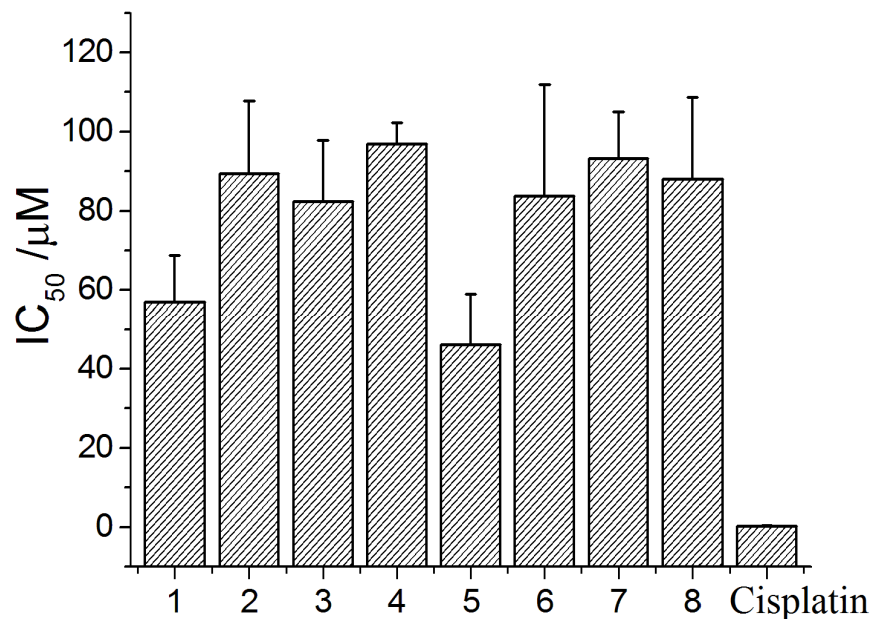


590 **Figure 3** (a) ORTEP diagram of complex  $[\text{Cp}^*\text{Rh}(\text{L4})\text{Cl}]\text{PF}_6$  (**7**) and (b) ORTEP diagram, of  
 591 complex  $[\text{Cp}^*\text{IrCl}(\text{L4})\text{Cl}]\text{PF}_6$  (**8**) with 50% probability thermal ellipsoids. Hydrogen atoms and  
 592 counter ions are omitted for clarity.

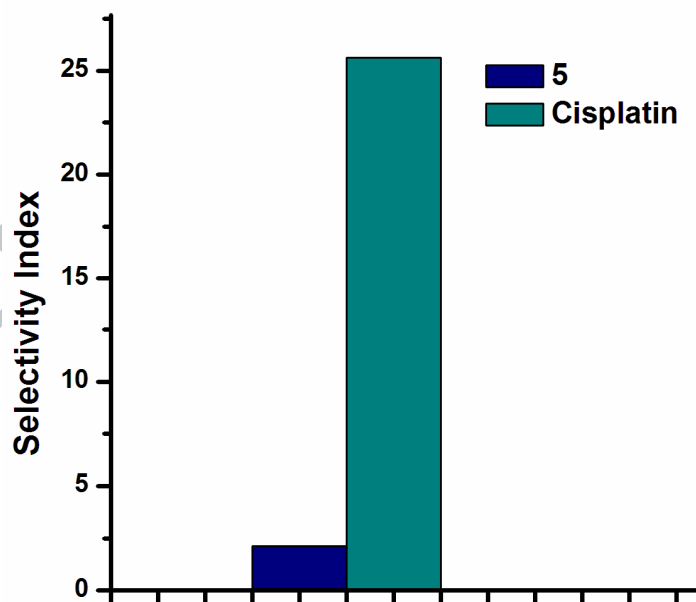


593

594 **Figure 4** Crystal structure of complexes (**3**) and (**4**) showing intramolecular hydrogen bonding.

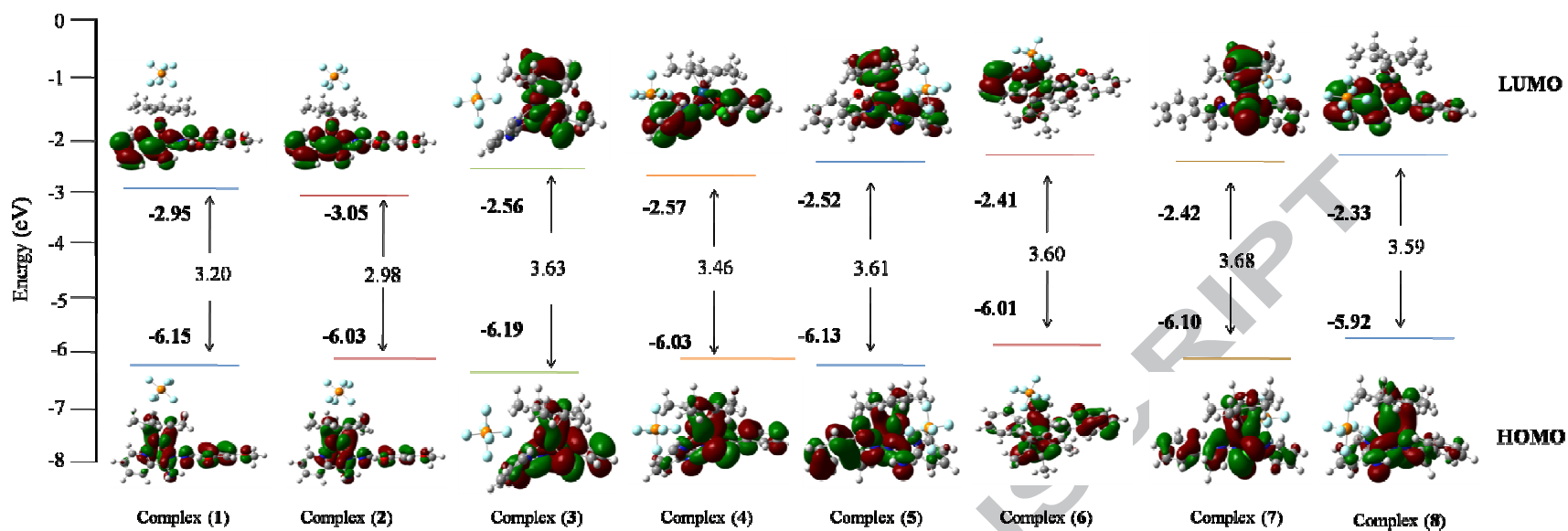


595  
 596 **Figure 5** Response of HT-29 (human colorectal cancer) to compounds (1-8) and cisplatin. Cell  
 597 were exposed to compounds (1-8) for 96 hours. Each value represents the mean  $\pm$  standard  
 598 deviation from three independent experiments.



599  
 600 **Figure 6** Graph showing selectivity index of complex **5** and cisplatin against HT-29 cancer cell  
 601 line. The selectivity index is defined as the IC<sub>50</sub> of ARPE19 cell divided by the IC<sub>50</sub> of tumour  
 602 cell line.





603

604

605

Figure 7 HOMO, LUMO energies and their energy gap of complexes (1–8)

606 Table 1. Crystal structure data and refinement parameters of complexes.

| Complexes  | [1] PF <sub>6</sub>  | [3] PF <sub>6</sub>  | [4] PF <sub>6</sub>  | [7] PF <sub>6</sub>   | [8] PF <sub>6</sub> Cl  |
|--|--|--|--|---|---|
| Empirical formula                                | C <sub>24</sub> H <sub>29</sub> ClN <sub>4</sub> O <sub>2</sub> F <sub>6</sub> PRh | C <sub>23</sub> H <sub>27</sub> ClF <sub>6</sub> N <sub>4</sub> OPRh | C <sub>23</sub> H <sub>27</sub> ClF <sub>6</sub> N <sub>4</sub> OPIr | C <sub>24</sub> H <sub>29</sub> ClF <sub>6</sub> N <sub>4</sub> PRh | C <sub>24</sub> H <sub>29</sub> Cl <sub>2</sub> F <sub>6</sub> N <sub>4</sub> PIr |
| Formula weight                                   | 688.84   | 658.82   | 748.11   | 656.84  | 781.58  |
| Temperature (K)                                  | 298(2)   | 293(2)   | 293(2)   | 293(2)  | 293(2)  |
| Wavelength (Å)                                   | 0.71073  | 0.71073  | 0.71073  | 0.71073   | 0.71073   |
| Crystal system                                   | triclinic  | monoclinic   | monoclinic   | monoclinic  | triclinic   |
| Space group                                      | <i>P</i> <i>T</i>  | <i>P</i> 2 <sub>1</sub> / <i>c</i>                                   | <i>P</i> 2 <sub>1</sub> / <i>c</i>                                   | <i>P</i> 2 <sub>1</sub> / <i>c</i>                                  | <i>P</i> <i>T</i>   |
| a (Å)/α (°)                                      | 8.3893(7)/89.370(6)  | 10.6710(6)/90  | 10.7019(5)/90  | 38.850(5)/90  | 7.9976(4)/87.496  |
| b (Å)/β (°)                                      | 10.5533(7)/86.439(6)   | 17.0730(8)/92.708(4).  | 17.0860(9)/93.062(4)   | 7.9488(5)/98.027(4)   | 12.4774(4)/82.086(4)  |
| c (Å)/γ (°)                                      | 16.6554(11)/71.182(7)  | 14.5390(8)/90  | 14.6118(9)/90  | 28.562(4)/90  | 14.6442(6)/72.596(4)  |
| Volume (Å <sup>3</sup> )                         | 1393.00(18)  | 2645.8(2)  | 2668.0(2)  | 1344.83(10)   | 1381.15(10)   |
| Z  | 2  | 4  | 4  | 2   | 2   |
| Density (calc) (Mg/m <sup>3</sup> )              | 1.642  | 1.654  | 1.862  | 1.622   | 1.879   |
| Absorption coefficient (μ) (mm <sup>-1</sup> )   | 0.836  | 0.874  | 5.231  | 0.857   | 5.148   |
| F(000)   | 696  | 1328   | 1456   | 664   | 762   |
| Crystal size (mm <sup>3</sup> )                  | 0.23 x 0.21 x 0.21   | 0.21 x 0.19 x 0.04   | 0.23 x 0.23 x 0.21   | 0.22 x 0.20 x 0.120   | 0.19 x 0.12 x 0.09  |
| Theta range for data collection                  | 3.174 to 28.654°.  | 3.33 to 26.73°.  | 3.31 to 26.37°.  | 3.386 to 28.842°.   | 3.23 to 26.37°.   |
| Index ranges                                     | -11<=h<=10, -12<=k<=13, -22<=l<=20   | -13<=h<=10, -10<=k<=21, -12<=l<=18                                   | -13<=h<=7, -21<=k<=19, -16<=l<=18                                    | -9<=h<=9, -12<=k<=22, -14<=l<=8                                     | -8<=h<=9, -15<=k<=15, -17<=l<=18  |
| Reflections collected                            | 10811  | 9506   | 10081  | 5614  | 7889  |
| Independent reflections                          | 6286 [R(int) =0.0717]  | 5375 [R(int) = 0.0268]   | 5422 [R(int) = 0.0277]   | 4000 [R(int) = 0.0268]  | 5335 [R(int) = 0.0296]  |
| Completeness to theta = 25.00°                   | 99.57 %  | 99.5 %   | 99.2 %   | 99.2 %  | 94.8 %  |
| Absorption correction                            | Semi-empirical from equivalents  | Semi-empirical from equivalents                                      | Semi-empirical from equivalents                                      | Semi-empirical from equivalents                                     | Semi-empirical from equivalents   |
| Refinement method                                | Full-matrix least-squares on F <sup>2</sup>  | Full-matrix least-squares on F <sup>2</sup>                          | Full-matrix least-squares on F <sup>2</sup>                          | Full-matrix least-squares on F <sup>2</sup>                         | Full-matrix least-squares on F <sup>2</sup>                                       |
| Data/restraints/parameters                       | 6286/0/362   | 2375/0/330   | 5422/0/340   | 4000/1/340  | 5335/0/349  |
| Goodness-of-fit on F <sup>2</sup>                | 1.197  | 1.063  | 1.026  | 1.041   | 1.046   |
| Final R indices [I>2σ(I)]                        | R1 = 0.0703, wR2 = 0.1706  | R1 = 0.0440, wR2 = 0.0895  | R1 = 0.0340, wR2 = 0.0630  | R1 = 0.0394, wR2 = 0.0822   | R1 = 0.0368, wR2 = 0.0875   |
| R indices (all data)                             | R1 = 0.0855, wR2 = 0.1772  | R1 = 0.0592, wR2 = 0.0968  | R1 = 0.0500, wR2 = 0.0683  | R1 = 0.0462, wR2 = 0.0858   | R1 = 0.0431, wR2 = 0.0912   |
| Largest diff. peak and hole (e.Å <sup>-3</sup> ) | 0.583 and -0.461   | 0.520 and -0.543   | 1.102 and -1.143   | 0.512 and -0.478  | 1.828 and -1.071  |
| CCDC No.   | 1477976  | 1477977  | 1477978  | 1477979   | 1477980   |

607 Structures were refined on  $F_0^2$ :  $wR_2 = [\sum[w(F_0^2 - F_c^2)^2] / \sum w(F_0^2)^2]^{1/2}$ , where  $w^{-1} = [\sum(F_0^2) + (aP)^2 + bP]$  and  $P = [\max(F_0^2, 0) + 2F_c^2] / 3$ .

608 Table-2. Selected hydrogen bonding distances (Å) and angles (°) of complexes **3** and **4**.

| Complexes | D-H····A           | H····A (Å) | D····A (Å) | D····H (Å) | ∠D-H··A(°) |
|-----------|--------------------|------------|------------|------------|------------|
| 3         | O(1)-H(1A)····N(4) | 1.916      | 2.638      | 0.820      | 146.39     |
|           | N(3)-H(3A)····N(4) | 2.323      | 2.624      | 0.860      | 100.76     |
| 4         | O(1)-H(1A)····N(4) | 1.908      | 2.634      | 0.820      | 146.90     |
|           | N(3)-H(3A)····N(4) | 2.328      | 2.629      | 0.860      | 100.78     |

609

610 Table-3 Response of HT-29 (human colorectal cancer) to complexes (**1-8**) and cisplatin. Each  
611 value represents the mean ± standard deviation from three independent experiments.

| Complexes | IC <sub>50</sub> (µM) |               |
|-----------|-----------------------|---------------|
|           | HT-29                 | ARPE-19       |
| 1         | 56.95 ± 11.76         | 85.31 ± 14.86 |
| 2         | 89.42 ± 18.33         | 93.45 ± 11.34 |
| 3         | 82.32 ± 15.55         | 83.03 ± 14.76 |
| 4         | 96.93 ± 5.31          | >100          |
| 5         | 46.17 ± 12.78         | 97.39 ± 4.53  |
| 6         | 83.74 ± 28.17         | >100          |
| 7         | 93.16 ± 11.84         | >100          |
| 8         | 88.09 ± 20.63         | >100          |
| Cisplatin | 0.25 ± 0.11           | 6.41 ± 0.95   |

612

613 Table 4. The energy gap, theoretical and experimental absorption bands, electronic transitions  
614 and dominant excitation character for various singlet states of the complexes (**1-8**) calculated  
615 with TD-DFT method.

| The most important orbital excitations | Calculated λ (nm) | Energy gap E (eV) | Oscillator strength (f) | Dominant excitation Character | Experimental λ (nm) |
|--|-------------------|-------------------|-------------------------|-------------------------------|---------------------|
| Complex ( <b>1</b> )                   |                   |                   |                         |                               |                     |
| H→L                                    | 417.16            | 3.20              | 0.2051                  | L1→L1(ILCT)                   |                     |
| H-2→L                                  | 359.64            | 3.53              | 0.0542                  | Cl→L1(LLCT)                   | 352.21              |
| H→L+2                                  | 355.41            | 4.03              | 0.0120                  | L1→L1(ILCT)                   |                     |
| H-4→L+2                                | 338.40            | 4.89              | 0.0139                  | L1→L1(ILCT)                   |                     |
| H-1→L+4                                | 278.91            | 4.73              | 0.0248                  | L1→L1(ILCT)                   | 276.0               |
| H-6→L                                  | 282.81            | 4.54              | 0.0073                  | L1→L1(ILCT)                   |                     |
| H-6→L+2                                | 275.41            | 5.37              | 0.0050                  | L1→L1(ILCT)                   |                     |
| H-11→L                                 | 235.62            | 5.08              | 0.0216                  | Rh→L1(MLCT)                   | 233.3               |
| H-5→L+4                                | 233.62            | 5.74              | 0.0480                  | Cl→L1(LLCT)                   |                     |

|             |        |      |        |                     |        |
|-------------|--------|------|--------|---------------------|--------|
| H-6→L+3     | 232.46 | 5.46 | 0.0105 | L1→L1(ILCT)         |        |
| Complex (2) |        |      |        |                     |        |
| H→L         | 462.76 | 2.98 | 0.0644 | Ir→L1(MLCT)         |        |
| H→L+3       | 358.38 | 4.64 | 0.0191 | Ir→Cp*(MLCT)        | 347.0  |
| H-4→L       | 340.55 | 4.01 | 0.0075 | L1→L1(ILCT)         |        |
| H-5→L+1     | 273.73 | 5.11 | 0.0470 | Cp*→L1(LLCT)        | 266.0  |
| H-2→L+4     | 266.79 | 5.33 | 0.1540 | L1→Ir(LMCT)         |        |
| Complex (3) |        |      |        |                     |        |
| H→L         | 532.04 | 3.63 | 0.0087 | L2→Rh(LMCT)         |        |
| H-2→L+1     | 348.95 | 4.11 | 0.0369 | L2→L2(ILCT)         | 344.10 |
| H→L+2       | 345.72 | 3.84 | 0.0128 | L2→Rh(LMCT)         |        |
| H-1→L+2     | 344.68 | 4.10 | 0.0089 | Cl+L2→Rh(LMCT)      |        |
| H-3→L       | 336.07 | 4.24 | 0.0047 | Cl→Rh(LMCT)         |        |
| H→L+4       | 289.42 | 4.85 | 0.0063 | L2→L2(ILCT)         | 286.1  |
| H-6→L       | 285.32 | 5.14 | 0.0163 | Cl+L2→Rh(LMCT)      |        |
| H-5→L+1     | 282.59 | 4.98 | 0.0391 | L2→L2(ILCT)         |        |
| H-4→L+4     | 237.16 | 5.74 | 0.0422 | L2→L2(ILCT)         | 234.30 |
| H-5→L+3     | 234.58 | 5.74 | 0.0161 | L2→L2(ILCT)         |        |
| Complex (4) |        |      |        |                     |        |
| H→L         | 444.09 | 3.46 | 0.0355 | L2→L2(ILCT)         |        |
| H-2→L       | 362.56 | 3.91 | 0.0077 | L2→L2(ILCT)         | 346.1  |
| H-1→L+1     | 332.29 | 3.80 | 0.0076 | Rh+L2→L2(MLCT/ILCT) |        |
| H→L+3       | 329.46 | 4.48 | 0.0468 | L2→L2(ILCT)         |        |
| H-4→L       | 324.35 | 4.53 | 0.0265 | Cl+Cp*→L2(LLCT)     |        |
| H-4→L+2     | 294.35 | 5.47 | 0.0164 | Cl+Cp*→L2(LLCT)     | 292.21 |
| H-1→L+2     | 288.71 | 4.74 | 0.0048 | Rh+L2→Rh+L2         |        |
| H-8→L+3     | 212.19 | 6.47 | 0.0387 | L2→L2(ILCT)         | 210.9  |
| H-6→L+4     | 210.71 | 6.56 | 0.0399 | Cl→L2(LLCT)         |        |
| H-2→L+5     | 210.22 | 6.26 | 0.0669 | L2→L2(ILCT)         |        |
| Complex (5) |        |      |        |                     |        |
| H→L         | 519.01 | 3.61 | 0.0076 | L3→Rh(LMCT)         |        |
| H-2→L+2     | 338.46 | 4.30 | 0.0120 | Cl→L3(LLCT)         | 332.0  |
| H-4→L+1     | 326.16 | 4.56 | 0.0052 | L3→Rh(LMCT)         |        |
| H-1→L+4     | 271.36 | 5.01 | 0.265  | L3→L3(ILCT)         | 268.0  |
| H-2→L+4     | 267.30 | 5.21 | 0.0177 | Cl→L3(LLCT)         |        |
| H-5→L+4     | 232.84 | 5.83 | 0.0498 | L3→L3(LLCT)         | 229.0  |
| H-10→L+2    | 229.44 | 6.14 | 0.0127 | Rh+L3→L3(MLCT/ILCT) |        |
| Complex (6) |        |      |        |                     |        |
| H→L         | 441.76 | 3.60 | 0.0160 | L3→L3(ILCT)         |        |
| H-2→L+1     | 334.33 | 4.45 | 0.0109 | Ir→L3(MLCT)         | 330.0  |
| H-1→L+1     | 328.24 | 4.33 | 0.1160 | L3→L3(ILCT)         |        |
| H-7→L       | 268.58 | 5.42 | 0.0159 | Ir→L3(MLCT)         | 256.0  |
| H-6→L       | 264.64 | 5.25 | 0.0304 | Cl→L3(LLCT)         |        |
| H-1→L+4     | 260.56 | 5.17 | 0.0350 | L3→L3(ILCT)         |        |
| Complex (7) |        |      |        |                     |        |
| H→L         | 518.07 | 3.68 | 0.0071 | L4→Rh(LMCT)         |        |
| H-1→L       | 448.90 | 4.05 | 0.0132 | Cl→Rh(LMCT)         | 400.0  |
| H-1→L+1     | 397.25 | 4.09 | 0.0148 | Cl→Rh(LMCT)         |        |
| H-1→L+4     | 269.94 | 5.23 | 0.0297 | Cl→L4(LLCT)         | 265.0  |
| H-2→L+3     | 262.52 | 5.20 | 0.0465 | Cl→L4(LLCT)         |        |

|             |        |      |        |              |       |
|-------------|--------|------|--------|--------------|-------|
| H→L+5       | 231.04 | 5.66 | 0.0547 | L4→L4(ILCT)  | 229.0 |
| Complex (8) |        |      |        |              |       |
| H→L         | 439.65 | 3.59 | 0.0196 | Ir→L4(MLCT)  |       |
| H-1→L+2     | 371.55 | 4.79 | 0.0381 | Ir→L4(MLCT)  | 361.0 |
| H-1→L       | 358.22 | 4.0  | 0.0349 | Ir→L4(MLCT)  |       |
| H-2→L+3     | 257.57 | 5.29 | 0.0359 | Cl→Cp*(LLCT) | 256.0 |
| H-4→L+3     | 255.65 | 5.61 | 0.0142 | L4→Cp*(LLCT) |       |

616

ACCEPTED MANUSCRIPT